NONLINEAR IMAGE RESTORATION
USING A
SEGMENTATION-ORIENTED EXPERT SYSTEM

by

Dong-Seok Jeong

Dissertation submitted to the Faculty of the
Virginia Polytechnic Institute and State University
in partial fulfillment of the requirements for the degree of
DOCTOR OF PHILOSOPHY
in
Electrical Engineering

APPROVED:

A. A. (Louis) Beex, Chairman

J. P. Bixler

R. W. Conners

R. V. Foutz

K. B. Yu

February 1988

Blacksburg, Virginia

NONLINEAR IMAGE RESTORATION
USING A
SEGMENTATION-ORIENTED EXPERT SYSTEM

by

Dong-Seok Jeong

A. A. (Louis) Beex, Chairman

Electrical Engineering

(ABSTRACT)

The implementation of a truly autonomous expert system for image restoration has been speculated for some time. It implies an attempt to combine two very unrelated fields, artificial intelligence and image restoration. The building of an expert system for image restoration can be justified as follows: 1) Although numerous image restoration techniques have been reported, there is no generally-agreed to best method. If one type of technique is applied to a class of images different from that for which it was designed, the results are often unacceptable. Rule-based expert systems can solve this conflict by choosing a correct method for each of a number of different cases, 2) Before building an expert system, we may need to check whether the system is suitable for our application or not. Forsyth has made a checklist of features that affect the suitability of the knowledge-based approach. Our application passed this suitability test. To the best of our knowledge no research work on this topic has been reported, in spite of this speculation and suitability.

Another important aspect of this research is the idea of applying the image segmentation concept to image restoration. We point out that segmentation and

sectioning (or partitioning) are different concepts. The sectioning concept has been used in image restoration for several different occasions. Few researchers have actually incorporated the segmentation concept into an image restoration method, realizing that the usual assumption of a single characterization for the whole image is not correct. We note that they use the same image restoration technique for each of the segments.

The goal of this research is to derive an automatic image restoration method which gives the best result in both quantitative and qualitative sense. It is achieved by building a segmentation-oriented rule-based expert system with the following major procedures: 1) Get a priori information either from the user or by computation, 2) Segment the image into several statistically homogeneous regions, 3) Select the most suitable image restoration technique for each segment with the help of the knowledge base and the inference engine, 4) Apply the selected methods to the corresponding segments, 5) Determine boundary region treatment.

Two image segmentation methods are installed in the system, which are applicable to most image models. The unified approach is good for images with a relatively small number of regions and the masking function approach is good for images with many details. Although a number of interesting methods for image restoration have been proposed, only a fraction of these are of practical use. About six image restoration techniques are installed into the system, along with programs to extract the a priori and a posteriori information. The merits of our proposed expert system include versatility, better performance, and modularity.

Acknowledgements

The first thank goes to Dr. A. A. (Louis) Beex for his valuable support from the beginning to final completion of this research. Without his guidance, this dissertation would not have been possible. I also give thanks to Dr. J. P. Bixler, Dr. R. W. Conners, Dr. R. V. Foutz, and Dr. K. B. Yu for their serving on my committee. I thank my parents for getting me off to a good start. Special thanks to the people who work and research in the Spatial Data Analysis Laboratory for their valuable support. They include Dr. R. W. Conners, the director of the Lab., , the system manager, and , the Gipsy manager. I thank the Lord for giving me the strength to persevere. To my dear daughter , I love you and thank you for tolerating your student father. Finally, no amount of words can express the love and appreciation I feel for my loving wife , who supported me all the way in spite of her busy schedule as a Ph. D. student and a consultant in EDRE.

Table of Contents

List of Illustrations

List of Tables

Chapter I. Introduction

1.1 Overview

Digital processing of images has been a very active field in the last two decades. One of the more active areas has been the digital restoration of images [1], as can be ascertained from several books, partly or exclusively on this topic [2,3,6,7,8,9,10,11,12,13,14].

The first fruitful application of digital image restoration techniques was the processing of images of the moon received from the unmanned craft that landed on the surface of the moon in the early 1960's [2, p.4]. Since that beginning, the interest in digital image restoration has continued to grow. New restoration methods are continuously being introduced. Therefore, anybody who enters this field for the first time could easily be intimidated by the large number of techniques published. It is one of the purposes of this research to summarize, compare, and classify those numerous techniques in a concise and simple manner.

By doing that, we can help researchers in their selection of restoration techniques suitable for their needs.

The implementation of a truly autonomous system for image restoration, such as an expert system, has been speculated for some time [3, p.75]. Such an expert system implies the combination of two very unrelated fields; artificial intelligence and image restoration. Although active research is being done in each of these two fields, no work has been reported to realize their interaction. In this dissertation, we will develop a versatile and general digital image restoration method with the help of a rule-based expert system.

The organization of this dissertation will be as follows. In the remainder of this chapter, we present the basic concepts which will be necessary to understand the subsequent material. In Chapter II, we present the historical background, and a survey of previous research related to digital image restoration. An attempt will be included to summarize those methods into a compact framework. We describe the new point of view on image restoration in Chapter III. This new point of view helps us develop a new restoration method. The implementation detail of this new approach is described in Chapter IV. We discuss performance criteria in Chapter V. Experimental results will be presented in Chapter VI. Finally, Chapter VII will conclude this dissertation with a summary and suggestions for further research.

1.2 Digital Image Restoration

A. Definition

An image formed either on photographic film or any other recording device is never a perfect replica of the spatial characteristics of the object [5]. Since physical imaging systems are not perfect, a recorded image will almost certainly be a degraded version of an original object or scene [7, p.216]. The degradation may be caused by such factors as spatial blur produced by the point spread function (PSF) of the imaging system; or nonlinearities in the recording/detecting device, to mention only a few [6 (p.266), 5 (p.1)].

The object of image restoration then is to obtain an estimate of an original image from data which has been degraded and recorded [6, p.266]. A simplified block diagram of an image restoration scheme is given in Figure 1 [7, p.216].

B. Image Formation/Detection/Recording

The image forms upon the human retina by the iris-lens portion of the human eye. Thus the eye embodies image formation systems (iris-lens) and image sensor or recording systems (retina).

According to the Webster dictionary (1985), the word image is defined as

" ... a reproduction or imitation of the forms of someone or something ... "

This dictionary definition is useful in conceptualizing an imaging system. Let us now have a close look at an imaging system.

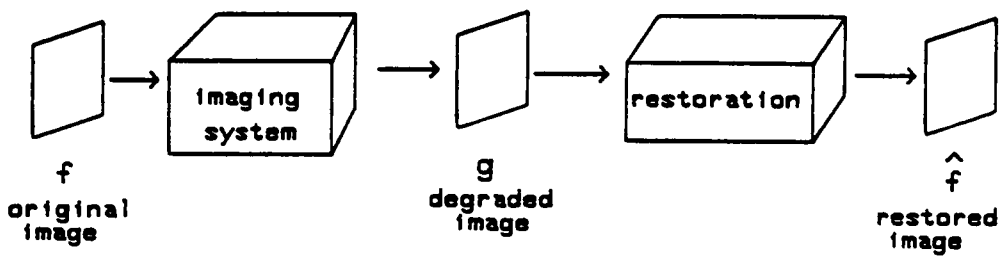

Figure 1. A simplified image restoration scheme.

Imaging System

The black box imaging system in Figure 1 can be described compactly by a canonic model [2, pp.23-25] that embodies the process of image formation, detection, and recording, including the existence of noise. The model is given below in Figure 2, where

$f(\xi, \eta)$: object plane radiant energy distribution,

h: point spread function of the image formation system,

$b(x,y)$: image plane radiant energy distribution,

s: detector response function; transforms image plane radiant energies into a response variable (usually nonlinear),

$r(x,y)$: response variable of detector; i.e. $r(x,y) = s\{b(x,y)\}$,

ε_1, ε_2: gain parameters; either 0 or 1,

ψ: feed-forward function to account for signal dependent noise,

n_1, n_2: noise processes,

n_3: resulting signal-dependent noise,

$g(x,y)$: response plus noise $= r_1(x,y) + n_3(x,y) + \varepsilon_2 n_2(x,y)$.

Image Formation

Let us next take a closer look at the image formation system. For simplicity, we assume a perfect detection/recording system. The schematic of image formation that results is shown in Figure 3 [2, p.9].

As seen in Figure 3, there is an object, $f(\xi, \eta)$, in the coordinate system (ξ, η), that is referred to as the object plane. The radiant energy reflected, transmitted, or emitted by the object propagates through space. An image formation

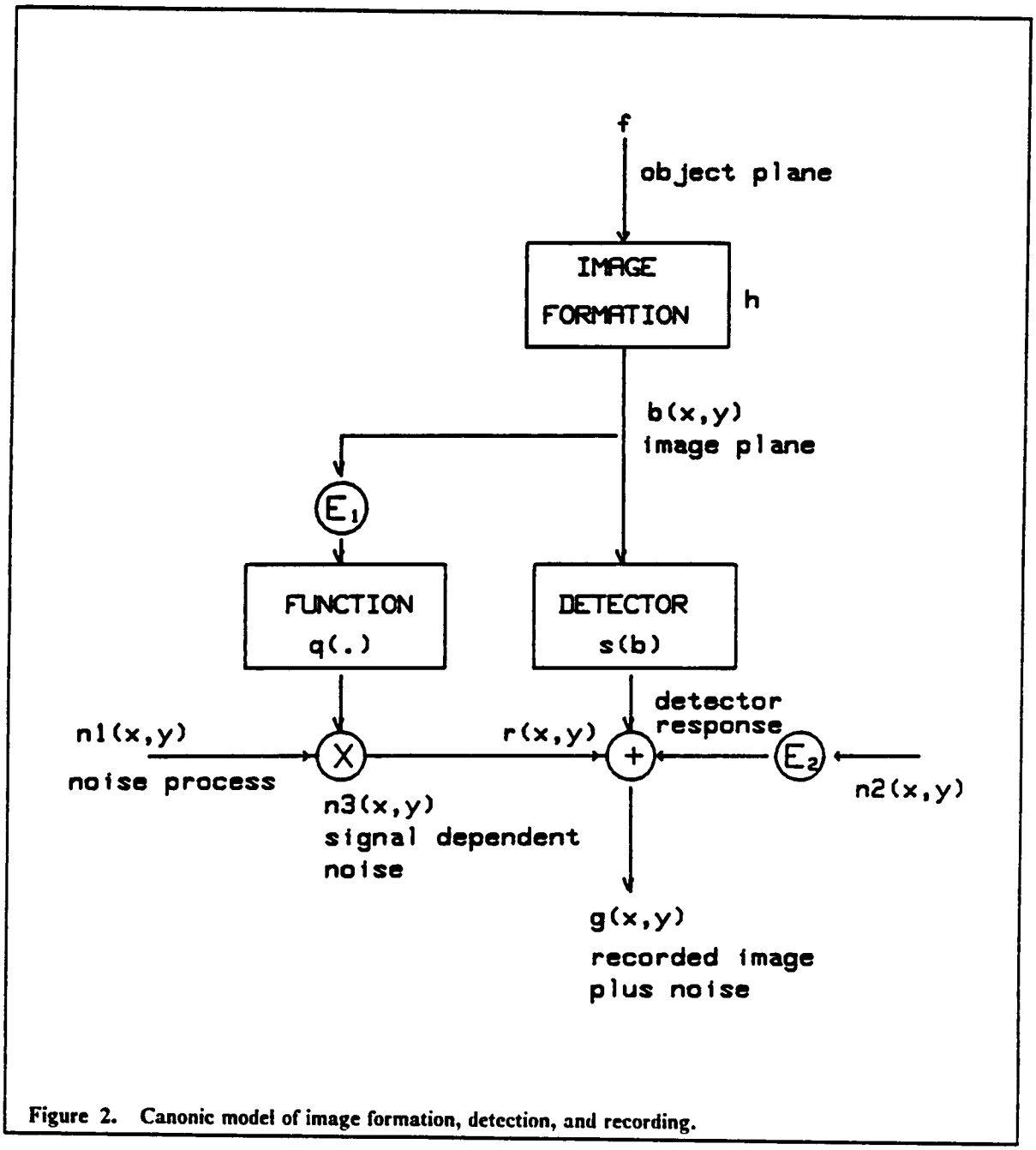

Figure 2. Canonic model of image formation, detection, and recording.

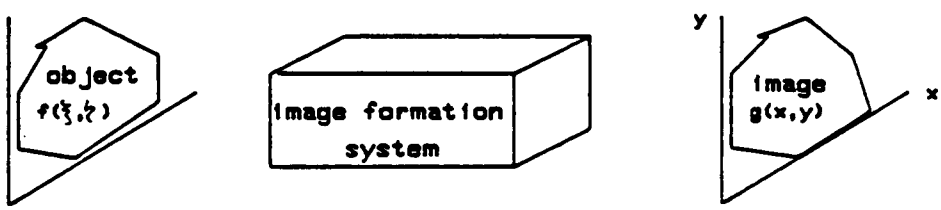

Figure 3. Schematic diagram of an image formation system

system intercepts the propagating radiant energy and transforms it in such a manner that in the coordinate system (x, y), which is referred to as the image plane, an image is formed [2, p.9].

There are three general principles upon which image formation is based; they are neighborhood processes, nonnegativity, and superposition [2]. Considering those three properties of the image formation system, we can express the general image formation equation as

$$g(x,y) = \int\int h(x,y,\xi,\eta,\ f(\xi,\eta))\, d\xi\, d\eta \tag{1}$$

Here the function h is known as the point-spread function (PSF) of the image formation system.

If the image formation system is linear, then

$$g(x,y) = \int\int h(x,y,\xi,\eta) f(\xi,\eta)\, d\xi\, d\eta \tag{2}$$

If the image formation system is linear and separable, then

$$g(x,y) = \int h_1(x,\xi) \int [\, h_2(y,\eta) f(\xi,\eta)\, d\eta]\, d\xi \tag{3}$$

Equation (3) shows the image formation process in terms of independent horizontal and vertical image formation.

If the PSF is space-invariant, then

$$g(x,y) = \int h(x - \xi, y - \eta, f(\xi, \eta))\, d\xi\, d\eta \tag{4}$$

If the PSF is linear space-invariant (LSI), then we have the familiar linear convolution,

$$g(x,y) = \int\int h(x - \xi, y - \eta) f(\xi, \eta)\, d\xi\, d\eta \tag{5}$$

Discrete Formulation

Even though the real scene is continuous, a discrete model is more useful for actual representation and computation using digital computers. Equation (2) can be rewritten in discrete form as

$$g_{ij} = \sum_{k=1}^{N} \sum_{l=1}^{N} f_{k,l}\, h_{i,j,k,l} \tag{6}$$

In matrix notation,

$$g = Hf \tag{7}$$

The PSF matrix H has interesting properties, depending on assumptions made [2], such as:

1. For a separable space-invariant PSF (SSIPSF):

$$H = A \otimes B, \text{ where } A, B \text{ are } \textit{Toeplitz}$$

2. For a nonseparable space-invariant PSF (NSIPSF):

$$H = \textit{Block Toeplitz}$$

3. For a separable space-variant PSF (SSVPSF):

$$H = A \otimes B, \text{ where } A, B \text{ arbitrary}$$

In the above, $\otimes$ is the direct or Kronecker product of matrices. For a nonseparable space-variant PSF (NSVPSF), no further simplification results.

C. Mathematical Representation

The basic model for the digital image restoration problem is

$$g = s\{Hf\} + n \tag{8}$$

where s is the sensor response operator, and n represents noise which we will assume to be signal independent. The problem then is to estimate the original image f given the PSF H, the recorded image g, and some a priori knowledge (usually of a statistical nature) about the noise n and/or the object f. We will examine this in more detail in Chapter II.

Ill-conditioned nature of restoration

One of the most essential problems is the fact that image restoration is an ill-conditioned problem at best and a singular problem at worst [2, p.113]. Assuming s is the identity function, we may get $\hat{f}$ by

$$\begin{aligned} \hat{f} &= H^{-1} g = H^{-1} (Hf + n) \\ &= f + H^{-1} n \end{aligned} \tag{9}$$

Examining Eq. (9), we see that the estimate is composed of two parts; the actual object distribution and a term involving the inverse acting on the noise. Here we can see two problems. The first is the lack of uniqueness of solution. Given the existence of a noise process, the multivariate sample vector n, there is a family of solutions. One must somehow select the proper solution from within an infinite family of candidate solutions. The second problem is the potential singularity associated with the inverse of the H matrix. If H is singular, there is no solution. If H is nearly singular, then the inverse H^{-1} will have very large entries, and consequently the term $H^{-1} n$ can dominate the solution f. There are a few other aspects to the ill-conditioned nature of restorations that we will not elaborate on, such as nontrivial perturbation effects on $\hat{f}$ by trivial perturbations in g, or non-uniqueness of $\hat{f}$ because of the randomness in noise processes [2].

D. Image Restoration versus Image Enhancement

Image restoration is closely related to image enhancement. When an image is degraded, restoration of the original image often results in enhancement. There

are however, some important differences between restoration and enhancement. In image restoration, an ideal image has been degraded, and the objective is to make the processed image resemble the original as much as possible. In image enhancement, the objective is to make the processed image better in some sense than the unprocessed image. In this case, the ideal image depends on the problem context and it is often not well defined. To illustrate this difference, note that an original, undegraded image can not be restored further, yet it can be enhanced; for example by increasing sharpness through high-pass filtering [3].

1.3 Expert Systems

A. Definition

Professor Edward Feigenbaum of Stanford University defined an expert system as follows [15]:

> " ... an intelligent computer program that uses knowledge and inference procedure to solve problems that are difficult enough to require significant human expertise for their solution. ... "

As stated above, an expert system is a computer system that encapsulates specialist knowledge about a particular domain of expertise and is capable of making intelligent decisions within that domain [16]. Feigenbaum defines those who build knowledge-based expert systems as knowledge engineers, and he refers to their technology as knowledge engineering. Early systems were usually called expert systems, but most knowledge engineers refer to their systems as knowledge systems.

Areas tackled successfully so far within an expert systems framework include medical diagnosis, geological exploration, organic chemistry and fault-finding in electronic equipment [16].

B. Architecture of Expert Systems

An expert system is typically rule-based or knowledge-based. The typical architecture of a knowledge-based expert system is given in Figure 4 [15]. The organization is slightly different from one author to another. The basic structure of an expert system is organized around two fundamental modules: the knowledge base and the inference engine [17]. The knowledge base can be structured in two parts: rules and facts. The rules contain the production rules in a procedural form, usually in "if-then" format. The facts contain the set of deductions performed during the activation of the system.

Notice that the inference engine stands between the user and the knowledge base. The inference engine performs two major tasks. First, it examines existing facts and rules, and adds new facts when possible. Second, it decides the order in which inferences are made. In doing so, the inference engine conducts consultation with the user.

C. Relation to This Research

R. Forsyth [16] has made a checklist of features which affect the suitability of the knowledge-based approach. As can be seen in Table 1, the field of image restoration falls more on the left than on the right. There have been several attempts to exploit the expert system concept in image understanding such as for

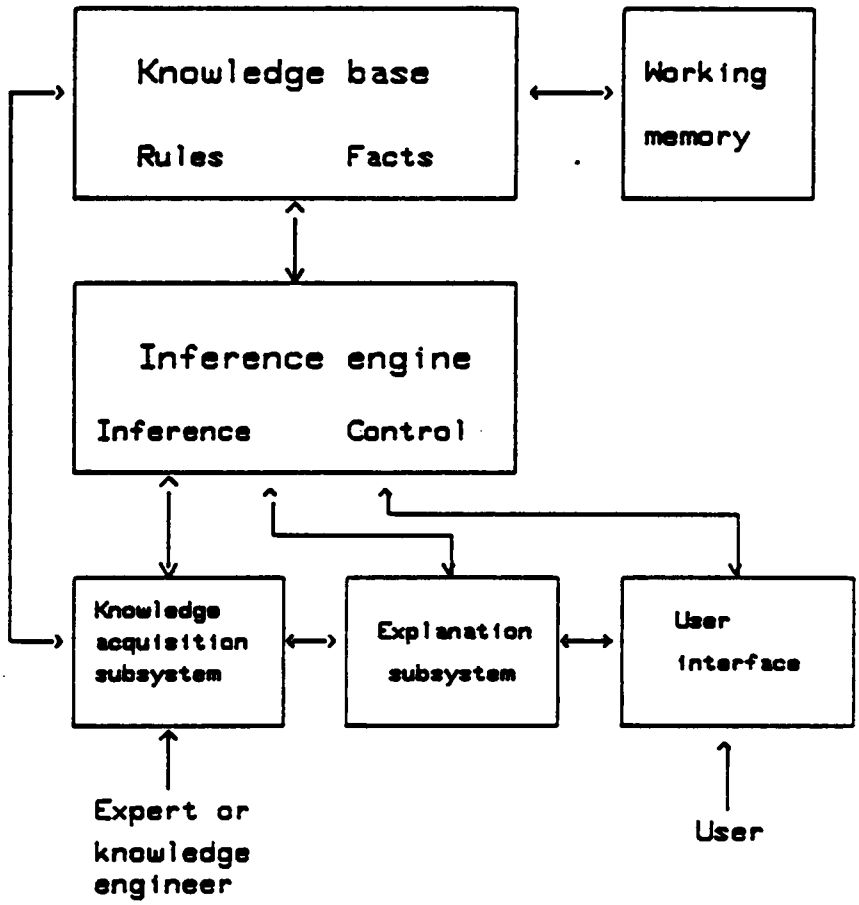

Figure 4. The architecture of a knowledge-based expert system.

Table 1. Checklist for the suitability of an expert system.

Suitable	Unsuitable
Diagnostic	Calculative
No established theory	Magic formula exists
Human expertise scarce	Human expertise is abundant
Data is noisy	Facts are known precisely

segmentation, interpretation, and surface representation [18,19,20,21,30]. To the best of our knowledge, however, no work has been reported in image restoration using that concept, even though a couple of authors express the necessity of using it [2,3].

1.4 Image Segmentation

A. Definition

Image segmentation is the division of an image into different connected regions each having certain properties, such as gray level or texture. Regions have two basic characteristics: 1) they exhibit some internal uniformity with respect to an image property, and 2) they contrast with their surroundings [11, p.223]. As a result of noise, the nature of these characteristics is not necessarily deterministic.

During the past two decades, many image segmentation techniques have been proposed. Likewise, numerous survey papers have been published [22,23,24]. The annual survey paper by Rosenfeld contains a rather complete bibliography of image segmentation research from 1972 through 1986 [25]. Broadly speaking, there are two ways of segmenting an image: by delineating the boundaries surrounding its regions, or by defining its homogeneous regions directly [26]. Obviously, if we can do one perfectly, we can also do the other perfectly. The processing methods used to determine the regions first are different however from the processing methods used to determine the boundaries first. Given a regional

property, such as intensity or texture, picture elements that are similar with respect to this property may be combined into regions. Alternatively, the borders between regions may be located by detecting discontinuities in image properties.

Another way of categorizing image segmentation techniques relates to the approach taken: pixel-based or region-based [25]. The pixel-based approach to image segmentation involves classification of the individual image points (pixels) into subpopulations. The segments obtained in this way are the subsets of pixels belonging to each class. The classification can then be done on the basis of intensity alone (thresholding), or on the basis of local properties derived from the neighborhood of the given pixel. An example of region-based segmentation methods is the split-and-merge approach suggested by Horowitz and Pavlidis [27]. Here the goal is to partition an image into homogeneous connected regions by starting with an initial partition and modifying it by splitting regions if they are not sufficiently homogeneous, and merging pairs of adjacent regions if their union is still homogeneous. In this approach, homogeneous might mean approximately constant in intensity or, more generally, it might mean a good fit to a polynomial of some degree greater than zero, as in the facet model [31].

B. Relation to This Research

Professors Haralick and Shapiro claimed in their survey paper [24]

> " ... there is no theory of image segmentation. Image segmentation techniques are basically ad hoc and differ precisely in the way they emphasize one or more of the desired properties and in the way they balance and compromise one desired property against another."

In this study, we want those image segmentation techniques which displays such desired properties as 1) versatility to handle most image models, including the facet (or polynomial) and the random-field (or texture) models, 2) producing relatively fast results, without iterations, and 3) boundary knowledge of the segmented regions does not have to be precise and clear. Image segmentation is not the final goal of this research, but instead it is a pre-processing step for the image restoration procedure. Moreover it is generally known that the noise in the vicinity of edges is less disturbing to the observer than noise in flat or homogeneous regions [34,35]. For this reason, errors introduced by unclear or abrupt boundaries are considered to be acceptable in this study.

To meet these three properties, we select the method proposed by Jeong and Lapsa [28,29]. The latter method uses a general decision criterion and can handle most image models. It uses a split-and-merge algorithm which satisfies the 2nd and 3rd requirements as well. The unified approach by Jeong and Lapsa is however not suitable for images with many details. For this reason, the masking function approach by Netravali and Brasada [34,56] is also selected, as an alternative segmentation tool.

Chapter II. The Science of Digital Image Restoration

2.1 Overview

Image restoration has been the subject of extensive research over the past two decades, as evidenced by the number of papers published on this topic. The research worker who enters the field of image restoration for the first time can easily be intimidated by the large number of techniques published [3, p.57].

Interestingly enough however, exclusive survey papers on this field have been rare, especially in recent years. More than a decade ago, Sondhi [36], Andrew [32], and Frieden [33] published survey papers on image restoration; in 1972, 1974, and 1975 respectively. Every digital image processing textbook devotes one chapter to image restoration [8,9,10,11,12,13], but they are all fairly introductory

and cover classical methods only. As even the recently revised editions [8,9] do not update contents to a large extent, textbooks do not provide updated and practical information to researchers in the field.

Probably the most practical and extensive source of digital image restoration has been a book by Andrews and Hunt [2] published in 1977. This book is wholly devoted to the science of digital image restoration. Even though this book is ten years old, it is still a useful source for the fundamental ideas of digital image restoration. A few tutorial papers have been published recently as a chapter of the book by Trussell [6], Biemond [7], and Hunt [3], but they fail to cover all branches of the reported work on digital image restoration.

In the remainder of this chapter, we try to classify most of the reported image restoration techniques into certain categories. By doing so, we can get a more unified and compact view of image restoration techniques. In Section 2, we review most of the reported work. Classification is made in a conventional way according to their approaches to image restoration. In Chapter 3, we examine image restoration methods from a different point of view, that will help us to develop a new restoration method in which we use the artificial intelligence concept.

2.2 Classification of Digital Image Restoration Techniques

Over the last few decades, many image restoration techniques have been proposed. Many of these techniques have been implemented and test results have been published. In this section, we survey these techniques, describe briefly the

underlying concepts, and discuss their merits, limitations, and applications. We then attempt to classify digital image restoration techniques, based on:

1) degradation models of the imaging system and the types of the noise it suffers
2) computational algorithms
3) availability of a priori information about the PSF and noise statistics
4) the number of channels (spectra) in the recorded image
5) specific applications

Of course there are special cases which can not be categorized this way, and those will be included under 5).

2.2.1 Degradation Models

Degradations may be divided into point degradations, spatial degradations, temporal degradations, chromatic degradations, or some combination thereof [2]. An alternative division is one into radiometric or geometric distortions [11]. Yet another division is by PSF; linear shift-invariant, linear shift-variant, or nonlinear. The nonlinear PSF is object-dependent, represented as follows

$$h = h(\xi, \eta, x, y, f(\xi, \eta))$$

The consequent nonlinear analysis does not lend itself to simple solutions. To help in understanding this concept, an example is given in [2]. Even though there are many imaging systems which exhibit an object-dependent PSF, such as X-ray

photos, only object-independent linear PSF models have been considered in the literature.

Point degradation does not incur blur in the images, but introduces a distortion due to coordinate transformations. That is

$$g(x,y) = h(x,y) f(p_1(x,y),p_2(x,y))$$

where $p_i(x,y)$ represents geometric coordinate transformations. Spatial degradation results when the PSF becomes a function of the object coordinate (ξ, η). In that case

$$h = h(x,y,\xi,\eta)$$

Spatial degradations introduce some form of smearing, or loss of resolution, to the image. Examples of spatial degradations are [2]; diffraction effects in optical systems; first, second, or higher-order optical system aberrations; atmospheric turbulence; motion blur; and defocused systems. Stated differently, spatial degradation is modeled by linear shift-invariant (LSIPSF) and linear shift-variant point spread functions (LSVPSF). An LSIPSF imaging system introduces the familiar convolution. The associated H matrix is block Toeplitz. Block Toeplitz matrices can be approximated with circulant matrices for which we can use FFT techniques [2].

Noise types may be classified as signal-independent or signal-dependent, additive or multiplicative, and white or colored. Typical examples of signal-dependent noise are film-grain noise (Gaussian type) and photo electronic shot

noise (Poisson type) [54]. The presence of these kinds of noise sources commonly leads to the use of nonlinear techniques. The approach of Kasturi and Walkup [37] is to transform signal-dependent noise into signal-independent noise, so that ordinary methods can be used. The correlation matrix for white noise is diagonal. It is due to this simplicity, that most reseachers assume the noise to be white. Stationarity of the noise process is also important, because otherwise the block-Toeplitz assumption would not be valid. In the majority of papers published on digital image restoration, the imaging system is assumed to be LSIPSF, with additive white noise. This is especially true in earlier papers.

Space-variant image formation was discussed by Lohman and Paris in 1965 [49]. Since then, several approaches were proposed to deal with space-variant degradations. The approach of Sawchuk [38] to space-variant motion degradation is based on the decomposition of the degradation into geometrical coordinate distortions and a space-invariant operation. Robbins [39] and Robbins and Huang [40] discuss the space-variant imaging system where the on-axis PSF is in focus and the off-axis PSF is spread out in radially symmetric. The algebraic approach, such as the iterative [41,43] or recursive [42,44,48] method, has been successfully applied to the problem of spatially-varying image degradation. The locally adaptive method is another way of solving the space-variant problem [45].

The recorded image is degraded by motion blur, whenever there is relative motion between an object and the imaging system. There are two kinds of motion blur: space-invariant and space-variant. Motion blur alone has generated a great deal of interest among researchers [38,46,47,48,50,51].

For an extremely defocused lens, the assumption can be made that the PSF is constant over the shape of the aperture, and zero elsewhere [11]. A defocused lens with circular aperture of radius a is modeled therefore with the following PSF, in polar coordinates [51]:

$$h(r) = \begin{cases} 1, & r \leq a \\ 0, & r > a \end{cases} \tag{10}$$

Note that the OTF (optical transfer function, Fourier transform of PSF) of (10) contains phase reversals.

The blur caused by atmospheric turbulence for long exposure times can be approximated by [52]:

$$h(x,y) = e^{-b(x^2+y^2)} \tag{11}$$

In this case, the OTF dose not exhibit phase reversals. McGlamery [53] discussed this in some detail.

2.2.2 Computational Algorithms

The published techniques have been organized in many different ways, according to the computational algorithms involved. Andrews and Hunt [2] made a distinction between non-iterative methods implemented by Fourier computation, and linear and nonlinear algebraic restoration methods. Hunt [3] simply

made a division into direct and indirect techniques. Trussell [6] characterizes on the basis of statistical information and constraints.

Our categorization here will be into Fourier based, algebraic, and contemporary methods.

a) Fourier Based Methods:

Fourier based methods are noniterative, and implemented by the use of Fourier computation. Results, such as a desired restoration, are produced in one step fashion by executing an appropriate spatial filtering operation. By assuming space-invariant imaging systems, we have a Toeplitz PSF matrix and a circulant approximation thereof. The result is, that discrete Fourier transforms (DFT) can be exploited in the computation.

The typical Fourier based filters are

a) the inverse filter, with a least-squares criterion,

b) the Wiener filter, with a MMSE criterion [65],

c) the homomorphic filter, with a power spectrum equalization criterion (also called spectral equalization filter) [63]

To describe the above filters in more detail, we start from the imaging model

$$g = Hf + n \tag{12}$$

where H is block Toeplitz and n is additive noise. The **inverse filter** meets the least-squares criterion by minimizing the norm of the noise term n. That is, we want to find

$$\hat{f} \text{ such that } n^T n = (g - H\hat{f})^T (g - H\hat{f})$$

Differentiating with respect to $\hat{f}$ and solving for $\hat{f}$ yields

$$\hat{f} = H^{-1} g \tag{13}$$

The solution (13) is called the inverse filter because the restoration is obtained with the inverse of H. As mentioned in Section I.2., the singularity of H and the effects of noise are of concern. For this reason, the inverse filter is applicable only to images with high SNR, i.e. very little noise. Another problem is the inversion of the large-size matrix. By approximating the block-Toeplitz matrix with a block-circulant matrix however, we can use a direct algorithm for computing the restoration by using DFT techniques [2]. The primary difference between the block-Toeplitz and block-circulant matrix is that they differ only by elements added to produce a cyclic structure in the rows. By approximating the block-Toeplitz with a block-circulant matrix, we approximate the linear convolution with the circular convolution. The larger the image size, the better the approximation will be.

A **Wiener filter** is derived from a criterion of minimum mean-square error (MMSE) between the original object distribution f and its estimate $\hat{f}$. That means we try to minimize the difference between f(x,y) and $\hat{f}(x,y)$ over some random ensemble of possible objects. Let $\hat{f} = L g$. Then we get

$$L = R_f H^T (H R_f H^T + R_n)^{-1} \tag{14}$$

where $R_f = E\{ff^T\}$, $R_n = E\{nn^T\}$.

Again, by approximating H, R_f, and R_n as block-circulant, we can use DFT methods to compute $\hat{f}$. See [2, p.137] for details. The estimate in the Fourier domain is [65],

$$\hat{F}(u,v) = \frac{H^*(u,v)\, G(u,v)}{|H(u,v)|^2 + S_n(u,v)/S_f(u,v)} \tag{15}$$

As can be seen in (15), there is no ill-conditioned behavior. Even though H(u,v) becomes small or even zero, the denominator can not fall below the lower limit set by the ratio S_n/S_f. With extremely low noise, such as $S_n \to 0$, this Wiener filter approaches the inverse filter. Note that we only need S_f and S_g in actual computation, where $S_g = S_f|H|^2 + S_n$.

In developing the filter, stationarity of the random process models is assumed. For models with underlying nonstationary random processes, the Fourier based computation methods are not necessarily valid. We must note that this MMSE estimate uses only the covariance information of the stationary model. It is generally known that the MMSE is not the criterion that the human visual system employs naturally. MMSE restoration in low SNR appears too smooth, the human eye is willing to accept more visual noise in exchange for the additional image structure lost in the process.

Exact information about the original object distribution being unavailable, it is reasonable to specify properties in terms of an average quantity, such as a power spectrum; which is a very common average quantity in signal processing.

The **homomorphic filter** [63] is derived by requiring the power spectrum of the estimated object $\hat{f}$ to equal the power spectrum of the original object f. That is, we require

$$S_f(u,v) = S_{\hat{f}}(u,v) \tag{16}$$

Then we get

$$\hat{F}(u,v) = \left| \frac{S_f(u,v)}{|H(u,v)|^2 S_f(u,v) + S_n(u,v)} \right|^{1/2} G(u,v) \tag{17}$$

As seen in Eq. (17), there is no ill-conditioned behavior in regions where H(u,v) $\rightarrow$ 0. The homomorphic filter approaches the square root of the signal-to-noise spectrum. The important point is that because the Wiener filter is forced to zero at a singularity, its frequency response shows greater variation than that of the homomorphic filter [3]. In addition, because of the cutoff behavior at a singularity, the power spectral equalization filter has higher gain at frequencies near the singularity, thus admitting more structure into the restored picture than the Wiener filter. Though it is not optimal in the MMSE sense, experimental studies show that a human viewer usually prefers images produced by power spectral equalization restoration over those restored by Wiener filtering [3]. Since the human visual system is not a minimum mean-square error processor, it is not a surprising phenomenon that the result of the Wiener filter is not necessarily preferred.

In general, the restoration for lower SNR with a homomorphic filter will appear slightly sharper than the corresponding Wiener filter restoration [3,64].

b) Algebraic Methods:

Algebraic methods for digital image restoration are based on the concepts of numerical analysis or linear algebra. These methods are more powerful and more flexible than the traditional ones based on spatial filtering using the two-dimensional Fourier transform. Such numerical methods can deal with problems concerning linear space-varying systems as well as linear space-invariant systems and can work under various constraint conditions. The typical algebraic methods may be classified as follows:

linear methods -
- inverse filter
- constrained least-squares filter
- parametric Wiener filter
- geometric mean filter
- pseudo-inverse filter

nonlinear methods -
- iterative methods
- Bayesian methods (MAP, ML)
- maximum entropy methods
- optimal recursive methods (Kalman)

In the **inverse filter** derivation, we seek the $\hat{f}$ that minimizes the norm of the difference between $H\hat{f}$ (the estimated object $\hat{f}$ reblurred through the PSF) and the given image g. The inverse filter is represented by

$$(H^{*t} H)^{-1} H^{*t} \tag{18}$$

where * stands for conjugation and t stands for transpose. Note that (18) has singularity problems if H is singular, as is the case with the traditional Fourier inverse filter.

A **constrained least-squares filter** has been developed by Hunt [66], in which the constraint allows the designer additional control over the restoration process. Let the linear operator, i.e. constraint matrix, be C. The constrained least-squares problem can then be formulated as

$$\text{minimize } ||Cf||^2 \text{ subject to } ||g - Hf||^2 = ||n||^2$$

By using the method of Lagrangian multipliers, we get

$$\hat{f} = (H^{*t}H + \gamma C^{*t}C)^{-1} H^{*t} g \tag{19}$$

Here γ, the reciprocal of the Lagrangian multiplier, must be adjusted such that the constraint $||g - Hf||^2 = ||n||^2$ is satisfied. This is often done in an iterative manner [66]. It is possible to generate a family of filters from (19) according to C.

If C = I, the identity matrix, it leads to the pseudo-inverse filter.

If C = eye model, the restoration is appealing to a human from a perceptual viewpoint [67].

If $C = \phi_f^{-1/2} \phi_n^{1/2}$, it leads to a parametric Wiener filter, where ϕ_f, ϕ_n are the signal and noise covariance matrices. If $\gamma = 1$, the filter reduces to the traditional Wiener filter.

The linear algebraic version of the Wiener filter minimizes the effective noise-to-signal ratio for the estimated object $\hat{f}$, while simultaneously minimizing the residual norm between the image and the reblurred estimated object. The resulting Wiener filter is given by

$$(H^{*t}H + \phi_f^{-1}\phi_n)^{-1} H^{*t} \tag{20}$$

With the constrained approach chosen, we get the **parametric Wiener filter**

$$(H^{*t}H + \gamma \phi_f^{-1}\phi_n)^{-1} H^{*t} \tag{21}$$

According to the value of γ, we can emphasize ($\gamma > 1$) or de-emphasize ($\gamma < 1$), the noise and signal statistics.

The motivation for developing the **geometric filter** is the desire to de-emphasize the low frequency dominance of the Wiener filter, while avoiding the singularity of the inverse filter. This can be done by parameterizing the ratio of the inverse filter to the Wiener filter effect on the restoration. That is

$$(\textit{inverse filter})^{\alpha} \ (\textit{parametric Wiener filter})^{1-\alpha}$$

where $0 \leq \alpha \leq 1$. By adjusting α and γ (of the parametric Wiener filter), we can get a number of different filters, such as the inverse filter, the Wiener filter, the geometric mean filter, the parametric Wiener filter, and all in-between filters, such as the inverse-dominated filter or the Wiener-dominated filter.

If the PSF matrix H is singular, there will be a possibly infinite number of objects $\hat{f}$ which could have provided the given g. A **pseudo-inverse filter** provides the object $\hat{f}$ which is smallest, and which when passed through H, also equals the image g. In other words, the pseudo-inverse filter is equivalent to minimizing the difference between the image g and $H\hat{f}$ (the estimated object $\hat{f}$ reblurred through the PSF), subject to a minimum norm on $\hat{f}$. The pseudo-inverse filter, denoted by H^+, is given by [69]

$$H^+ = \lim_{\gamma \to 0} (H^* H + \gamma I)^{-1} H^{*t} \tag{22}$$

A major problem associated with algebraic image restoration methods is the problem of solving simultaneous equations with many unknowns (an image of 200 x 200 pixels has 40,000 unknowns). In practice, it is impossible therefore to solve them directly or by using the inverse matrix, even when a large computer is used. The requirement of a large memory is another problem.

Iterative methods form one approach to solve the above problems. The use of an iterative method saves much computer memory and much computation time if the PSF matrix H is sparse [71], which is generally the case, because the extent of the PSF in the actual imaging system is considerably smaller than that of the object. Iterative techniques are also flexible in incorporating a priori in-

formation into the restoration process, and they have become popular in image restoration because of this flexibility. There are a number of iterative techniques, such as the Jacobi method, the Gauss-Seidel method, the steepest descent method [70], and constrained iterative restoration methods [71] [72]. Singh et al. [73] published a good survey paper on this topic.

Convergence is the important factor in judging the performance of iterative techniques. During iterations, several constraints can be introduced. Convergence of the iteration is guaranteed, when the composite constraint operator is nonexpansive. Schafer et al.[72] and Trussell [74] discuss convergence issues in detail.

The **maximum a posteriori density (MAP) method** uses Bayes theorem to express the conditional probability that any restoration $\hat{f}$ is correct, given a blurred image. The criterion can be written as follows

$$\underset{f}{maximize}\ p(f|g) = \frac{p(g|f)\,p(f)}{p(g)} \tag{23}$$

As seen in Eq. (23), the form of the density functions must be known. An exponential form is usually assumed for both p(g|f) and p(f) [6]. The form for p(g) does not matter since the term is independent of f, and thus its derivative with respect to f will be zero. While many exponential forms can be selected, the most common is the multivariate Gaussian distribution [6]. Assuming image formation models with sensor nonlinearity s(.),

$$g = s(Hf) + n \tag{24}$$

we obtain the following implicit equation in $\hat{f}$,

$$\hat{f} = \bar{f} + R_f H^t S_b R_n^{-1} (g - s\{H\hat{f}\}) \tag{25}$$

where $\bar{f}$ is the mean of the distribution of f, S_b is a diagonal matrix of derivatives of s evaluated at the points of $b = H\hat{f}$. A numerical solution to Eq. (25) can be obtained by using the modified Picard method [77], which is however computationally expensive. If the function s is a linear transformation, the matrix S_b becomes an identity matrix. By the use of circulant approximations for R_f, H, and R_n , the MAP estimate can be approximately computed by using the efficient FFT. It is known [75] that the MAP and MMSE estimates are equivalent for linear systems and symmetric densities.

It has been shown that the more exact model leads to restorations which are superior to those obtained by simpler assumptions [76]. However, the computational burden may be orders of magnitude greater. A reasonable strategy is to obtain a restoration by a fast linear method, such as the Wiener filter or linear MAP, and to observe whether this result is adequate. If not, the more expensive nonlinear technique may be applied. Cannon et al. [64] suggest that the result of the Wiener or PSE restoration be used as the starting point for the numerical MAP method. They conclude that for focus-blurred images, the MAP method performs better than other methods, such as the Wiener or PSE method, especially in a high SNR environment. The MAP method appears to be better able to cope with the singularities and phase reversals (of that type of blur) [64]. The

MAP filter passes more high-frequency information, including noise, than the MMSE filter [6]. This often results in visually more pleasing images.

Associated with the MAP estimate is the **maximum likelihood (ML) method**, which is derived by assuming that p(f|g) = p(g|f); i.e. the vector f is a nonrandom quantity. The maximum likelihood estimate is then given by [2]

$$\hat{f}_{\mathrm{ML}} = H^{-1} s^{-1}(g)$$

It is seen that the ML method requires the inverse transformation of the sensor response, and also that we have potential problems associated with the ill-conditioned nature of H^{-1}. Precisely because of these problems, the ML method is of limited utility [2].

Suppose that the object f is normalized to unit sum, that is $\sum_i f_i = 1$, so that the scalar values f_i can be interpreted as probabilities [68]. The entropy of the object would then be given by

$$\text{entropy} = -\sum_i f_i \ln f_i = -f^T \ln f \tag{26}$$

By applying a constrained least-squares approach with the constraint $||g - Hf||^2 = ||n||^2$, the following relation [2, p.153] results

$$\hat{f} = \exp\{-1 - 2\gamma H^{*t}(g - H\hat{f})\} \tag{27}$$

This is a nonlinear matrix equation for $\hat{f}$, where the exponential guarantees the positivity of the restoration. Linearization, by observing the first two terms in the Taylor series expansion, results in

$$\hat{f} = (H^{*t}H + \gamma I)^{-1} H^{*t} g \tag{28}$$

where γ is the reciprocal of the Lagrangian multiplier. The formulation in Eq. (28) is known as the linearized maximum entropy filter. Actually there are two forms of the **maximum entropy method** [6]. The first is derived from a maximum likelihood assumption [68]; the second from a maximum a posteriori assumption [2,78]. Eq. (27) is derived by the second assumption. While the forms of the two maximum entropy solutions may seem quite different, they very much have the same characteristics.

The maximum entropy method works well with an image having relatively few high values, and with little correlation between points. A starfield from astronomical imagery fits this requirement well.

In recent years **recursive Kalman filter** techniques have been applied to the area of image restoration in hopes of obtaining an optimal restoration method. The first attempt to extend Kalman filtering to the processing of image data was performed by Nahi and Assefi [79]. Even though the observed image is a two dimensional array, it was treated as one dimensional by scanning the image line by line and applying a Kalman filter. A common problem encountered in designing two-dimensional recursive filters is the lack of a 2-D spectral factorization theorem. Habibi [115] was the first to generalize Kalman filtering to two dimen-

sions. His filter was essentially a one-step predictor. Aboutalib and Silverman [46] discuss linear motion blur, which they then extended to the case of general motion blur in Aboutalib, Murphy, and Silverman [48]. Woods and Ingle [80] derive a Kalman filter for scalar observations based on a nonsymmetric halfplane model for the original image. The image is filtered one pixel at a time. Murphy and Silverman [81] discuss a vector Kalman filter based on a general semicausal image description. This filter processes the image one line at a time.

All approaches with two-dimensional recursive filters are characterized by large computational and storage requirements, and complexity in design and implementation. For these reasons many authors propose various modified recursive Kalman techniques which are suboptimal in performance, but which reduce computational load and memory space requirements. Some references are Rajala and Figueiredo [35], Biemond, Rieske, and Gerbrands [81], Watanabe, Osaki, Horii, and Kageyama [82], Felix, Cheng and DeMoment [88], and Min and Xiang [83]. The recursive filters are most useful when the degradations are causal and spatially varying.

A compromise, between the transform based Wiener filters and the two dimensional recursive filters, is obtained by the semicausal filters [84]. These filters are implemented by taking an image transform along one of the coordinates and performing recursive filtering operations on the other coordinate. These filters combine the advantages of recursive and transform based algorithms.

Due to the nonrealistic assumption that only a few parameters, such as correlation coefficients in x and y, can embody the features of interest in a typical

image, the results obtained with real images are often disappointing. A better assumption would be that there are different regions in an image where different correlation coefficients would apply. This problem is alleviated by partitioning the image into regions according to some criteria, local spatial activity [35] for example. The restoration process is then linear within segments, but nonlinear considering the whole image.

C) Contemporary Methods:

Two recently proposed methods will be discussed here. They are projection on convex sets (POCS), and fuzzy set methods.

POCS Methods

The constrained approach discussed earlier in this section emphasizes a single constraint, forcing the norm of the residual to be equal to the variance of the noise. There may be other constraints which are desired, but additional constraints may result in an unwieldy set of equations [6]. A new approach is to formulate the constraints as convex sets. Youla [94] applied this concept to image restoration by a method of alternating projections. He considered the image restoration problem as that of determining an original signal f in a Hilbert space from the projection of that signal onto a subspace. The alternating projection algorithm provides background for its extension that can be applied to image restoration. The restriction of defining subspaces can be broadened to that of requiring closed convex sets [85, 86]. A set C, is convex if for any two points in

C, the line between the points is also in C. That is, if x_1 and x_2 are in C, then the point $x = \alpha x_1 + (1 - \alpha)x_2$ is also in C for all $\alpha, 0 \leq \alpha \leq 1$. A set C, is closed if the limit point of any sequence of points in C is also contained in C. That is, if x_i is in C for all i and $||x - x_i|| \rightarrow 0$ as $i \rightarrow \infty$, then x is in C.

Constraints can be applied to the image restoration problem by formulating them as closed convex sets. Youla and Webb proposed and proved 11 different closed convex sets [85]. Sezan and Stark actually applied some of them to the restoration problem [86,87]. This represents a novel method of including a priori knowledge in the restoration process. Each closed convex set represents a constraint on the image. The original signal must then lie in the intersection of all the sets,

$$f \in \bigcap_{i=1}^{m} C_i$$

where C_i is a closed convex set. Beex [119,120] proposed a similar concept for noisy data. The solution algorithm is to sequentially project the estimates onto each of the sets until an estimate $f^{(k)}$ is found in the intersection. The method can be described mathematically by

$$f^{(k+1)} = \left(\prod_{i=1}^{m} P_i\right) f^{(k)} = P_m P_{m-1} \cdots P_1 f^{(k)} \tag{29}$$

where P_i is the projection operator onto the ith closed convex set C_i. The projection of a vector x onto the closed convex set C is the vector $x_c \in C$, which is closest to x; that is, $||x - x_c||$ is a minimum. The initial estimate $f^{(0)}$ can have a profound effect on the restoration result [89]. This indicates that the initial estimate $f^{(0)}$ may be useful in allowing the user to insert a priori knowledge [89, 90]. The initial estimate should be chosen to have the characteristics of the true solution.

Leahy and Goutis [91] pointed out that the POCS method is suboptimal and has two major problems; slow convergence and nonuniqueness of the solution. They proposed a new technique, so called dual optimization, for finding an optimal feasible solution which is free from the above mentioned problems. The dual optimization procedure however, does not offer the full flexibility of POCS in that the number of constraint sets is limited [91].

Fuzzy Set Methods

The latest entrance into the world of image restoration methods is the application of the theory of fuzzy sets proposed by Civanlar and Trussell [92]. The theory of fuzzy sets is a relatively new but well-developed mathematical area which is beginning to find application in such areas as operations research and economics. The theory provides a tool for handling inexact or approximate knowledge.

As an example, we can look at the following closed convex set [90,119]

$$C = \{f \mid \|g - Hf\|^2 \leq \sigma_n^2\} \tag{30}$$

where σ_n^2 is the noise variance. The fact that C is convex can be shown easily. Since the value of σ_n^2 is estimated, there is some uncertainty about its value. The true solution could lie outside of the set C. Some values are more likely than others, and values outside the range are not impossible. A more accurate constraint on the solution of the restoration problem should reflect this uncertainty. Fuzzy set theory accommodates this uncertainty by the value of the membership function. The membership function [93] describes the strength of our belief that an element x is a member of the set A, and is denoted by $\mu_A(x)$. If $\mu_A(x) = 1$, we are certain x is in A; if $\mu_A(x) = 0$, we are certain that x is not in A.

A fuzzy set A is defined on a set of objects Ω as a set of ordered pairs

$$A = \{x, \mu_A(x)\}, \quad x \in \Omega \tag{31}$$

where $\mu_A(x)$ is a membership function of the set. The function $\mu_A(x)$ is defined over all x in the space Ω and has a value between 0 and 1.

Fuzzy sets can be used to describe constraints for restoration problems. Thus, as with the POCS method, the solution is a vector in the intersection of a specified collection of fuzzy sets. It is natural to define the solution as that member which best satisfies all of the imposed constraints. That is

$$\underset{x}{maximize} \{ minimum \ (\mu_{A_1}(x), \ \ldots, \ \mu_{A_N}(x))\} \tag{32}$$

The methodology for solving the maximization problem will depend on the particular mathematical forms of the membership functions [6].

The key to the use of fuzzy sets is the membership function. The membership function may be equivalenced to a probability density function. If the distribution of x is known, that function can be used to define a membership function [94]. A fuzzy set is defined by its membership function. Therefore the user must mathematically describe the qualities he desires in the restored image. Some of the common examples include positivity, smoothness, and maximum power [92,119]. Some other qualities are also suggested [6]. Often it is difficult for the user to define a membership function describing the quality he desires. It is recommended that care be taken to choose a form that permits a tractable numerical solution [6].

This fuzzy set approach to image restoration is in its infancy. Preliminary work with one dimensional signals has shown some promise [6, 92]. A critical drawback of this method is the fact that the computational requirements are quite heavy. This has limited the dimensionality of the problem. At present it appears that numerical solutions to the fuzzy set formulation will have to be developed on a case by case basis. Another problem is the dependence of the solution algorithm on the choice of membership functions and the defining algebra.

2.2.3 Availability of A Priori Information

According to the availability of a priori information about the PSF and noise statistics, the published techniques may be organized into four groups. These are the combinations of (un)known PSF and (un)known noise statistics. Most image restoration methods are based on the assumption that the correct PSF and noise statistics are available a priori. Most restoration methods discussed in Subsection 2.2.1 fall into this category.

If the **noise statistics are unknown**, they are estimated from the given image. The noise norm is a very popular statistic in constrained restoration methods. Most constrained restoration methods use the constraint requiring the norm of the residual image to be equal to the noise norm. If we follow the general assumption of white Gaussian noise, then the norm of the noise is the same as its variance. In Eq. (30), the noise variance was used to define a convex set. The noise variance can also be used to define the convergence criterion for the iterative restoration method.

Noise variance can be calculated from the regions of relatively unchanging object content. By comparing the eigenvalue plot of a dark flat region to that of a light flat region, we can tell whether the noise is signal-dependent (multiplicative) or not [2, p.102]. It is believed that the noise is multiplicative, or at least has a signal dependent component, if the noise process changes as a function of the underlying object brightness.

Kondo and Atsuta [95] proposed a restoration method which does not need the noise norm information. They proposed two quality measures for a restored image; a measure of smoothness and a measure of fidelity. A measure of fidelity has the same role as the noise norm in the constrained least squares method.

If the **PSF is unknown a priori**, we have two choices. We may use those image restoration methods which do not require PSF information, or we may derive the PSF characterization from the degraded image.

The homomorphic filtering method does not require the PSF information a priori. As discussed in Subsection 2.2.2, the power spectrum of the PSF is estimated from the image and used for image restoration.

The method of deriving the PSF from the analysis of points or lines in the image has been successfully applied in a wide number of cases [2, 6, 96, 97]. A point image, such as the image of a glint of sunlight off glass or metal, is by definition the point spread function. On the other hand, the image of an edge is the projection integral of the PSF in the direction of the edge. In this case an additional assumption, such as rotational symmetry, is required to recover the PSF from the line spread image, which may be observed in the image itself.

Quite recently a number of researchers, including Biemond [98], Woods [62,98], and Kaufman [62], reported their work on identification of PSF parameters. The blurred image is modeled as the output of a noncausal unknown linear system, which is characterized by its PSF. Tekalp, Kaufman, and Woods [62] developed spatial-domain procedures for simultaneously identifying both the PSF parameters and the image model parameters without assuming a specific func-

tional form for the PSF. The image model coefficients define the AR part, and the blur parameters define the MA part. The identified parameters are then used for the design of a two-dimensional reduced update Kalman filter for subsequent restoration of blurred and noise image.

Biemond, Putten, and Woods [98] propose a parallel scheme for the identification of two-dimensional noncausal image blurs. They formulate the blur identification problem as a parallel set of one-dimensional nearly uncorrelated ARMA identification problems. Again the image model coefficients form the AR part and blur parameters form the MA part. They express the ARMA models as equivalent infinite-order AR models, and then follow the linear estimation procedure developed by Graupe, Krause, and Moore [99]. They extend this procedure by developing a parallel Kalman restoration filter with those identified image model and blur parameters [61]. Han and Yenping [47] also report a method for estimation of the motion blur parameters. They propose a new degradation model for motion blur and apply sign statistics to estimate the degraded parameters.

2.2.4 The Number of Channels

Based on the number of channels, image restoration techniques can be grouped into single or multi-channel image methods. By single channel images, we mean monochrome images. Multi-channel (or multi-spectrum, multi-plane)

images are defined as images with multiple image planes obtained by an imaging system that measures the same scene using more than one type of sensor.

Digital image restoration of monochrome images has been studied extensively; the restoration of multichannel images however, has received attention only recently [100,101,102,103,104]. Most of the restoration techniques for multi-plane images so far involve individual image plane restoration, without using the interactions between the image planes. Hunt and Kubler [103] however, propose a multichannel restoration scheme based on the assumption that the signal autocorrelation, the between-channel and within-channel relationship, is separable. This leads to a linear transformation to decorrelate the signal between image channels, making the channels orthogonal. Galatsanas and Chin [102] do not introduce the assumption of spectral and spatial separability in their restoration algorithm. They use both the within-channel and between-channel correlation. They claim that as a consequence, the restored image is a better estimate than the one produced by independent channel restoration. Angwin and Kaufman [104] also consider multichannel image restoration by applying the reduced update Kalman filter to each of the red, green, and blue components of a color image.

Chapter III. Hierarchical Classification of Image Restoration Methods

We will next classify reported work according to the number of restoration methods involved for a single degraded image, and the shape of the degraded images to be processed. A division can be made into four categories, which in increasing order of intelligence are the following

(1) a single method for one image with single region

(2) a single method for one image with sectioned regions

(3) a single method for one image with segmented regions

(4) multiple methods for one image with segmented regions

We note that categories (1), (2), and (3) are special cases of category (4). This evolution concept is illustrated in Figure 5.

Examining restoration methods in this way, we realize how research has been heavily concentrated in one direction. Almost all of the reported restoration

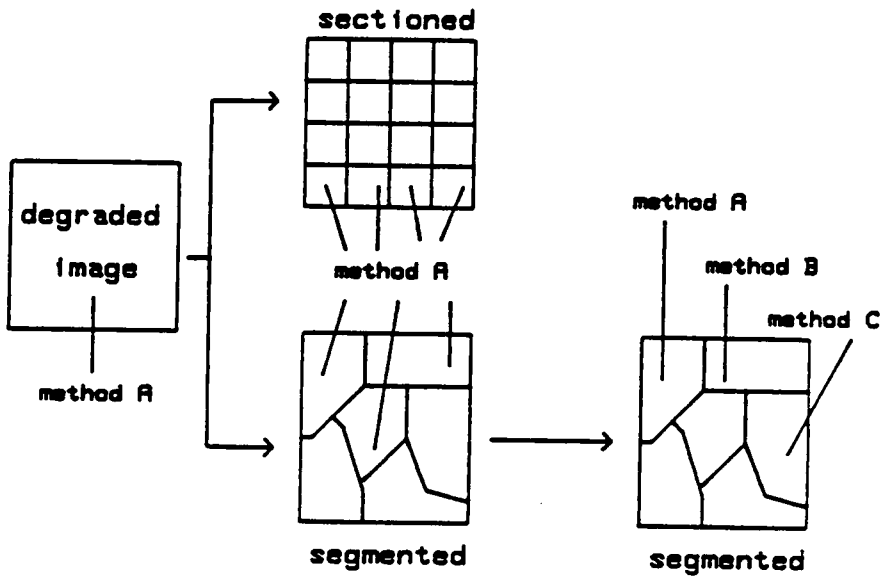

Figure 5. Evolution of image restoration concepts.

algorithms apply a single method to the whole picture, falling into category (1). These restoration methods were covered in Chapter II, which we refer to for a discussion of category (1).

The sectioning concept has been used in image restoration mainly for reducing the computational burden. Sectioning is the division of an image into equal-sized regions. By processing small portions of an image separately, the requirement for computer memory space is reduced. A few papers [44,45,55] fall into category (2).

We point out that segmentation and sectioning are different concepts. Segmentation is the division of an image into different connected regions each having certain properties, such as gray level or texture. Actually image segmentation alone is one of the major fields within the image processing discipline. If we have a degraded image of a building with a grassy field in the background, the usual assumption of a single characterization for the whole image is not correct. The correlation among pixels of the building is different from that of the grassy field. In this case, it is advisable to segment the image into two regions so that we can use different parameters for the different regions. Image segmentation will not only reduce the computational load and memory space, but it will also improve overall performance. As a result of processing the segmented regions separately, we get a nonlinear restoration effect for the whole image even when each of the segmented regions is processed by a linear method. This idea was speculated a decade ago [2], but no work has been reported until recently. Rajala and

Figueiredo [35], and Jinchi et al. [57], proposed image restoration methods in which segmentation is required. The latter belong to category (3).

To the best of our knowledge, no reported image restoration method falls into category (4). Even though it is not about image restoration, the paper by Qian et al. [58] on image enhancement is worth mentioning here. This algorithm includes segmentation and four different filters. It applies different filters for regions with different local activities. The proposed research falls into category (4). We segment the image into regions of homogeneous characteristics. For each of the different regions, we decide the most appropriate restoration technique with the help of a rule-based expert system. Details will be discussed in the next chapter.

Chapter IV. Image Restoration Using a Knowledge System

4.1 Overview

In this research, we plan to develop a general and versatile digital image restoration tool with the help of a segmentation-oriented rule-based expert system. We would like to emphasize a few points to justify the idea of building an expert system for image restoration.

Though numerous image restoration techniques have already been reported, there is no generally-agreed to best method. Most methods are designed to treat a very specific case. If one type of technique is applied to a class of images different from that for which it was designed, the results are often unacceptable [6]. Rule-based expert systems can resolve this conflict by choosing a correct method

for each of a number of different cases. In fact Hunt [3, p.75] has already speculated the necessity of an expert system in this field [3, p.75].

> " ... The implementation of a truly autonomous system for image restoration will probably require integration of restoration filters with knowledge base or expert systems of artificial intelligence. ... "

Before building an expert system, we may need to check whether such a system is suitable for our application or not. As given in Table 1 of Chapter I, R. Forsyth [16] has proposed a checklist of features that affect the suitability of the knowledge-based approach. According to Forsyth, if our intended application falls more on the left than on the right of this table, we should seriously consider an expert system. Our application passed this suitability test. To the best of our knowledge no research work on this topic has been reported, in spite of this speculation and suitability.

Another important aspect of our research is the idea of applying the image segmentation concept to image restoration. This idea was proposed by Hunt [2, pp.204-206] to derive the optimal recursive estimates of the original image consisting of several different regions. This idea however, was only speculated, and not implemented until recently.

Segmentation and sectioning (or partitioning) are different concepts. The former process is done with intelligence, whereas the latter is done blindly (without intelligence) by dividing the image into equal-sized blocks. The sectioning concept has been used in image restoration on several different occasions. In the homomorphic filtering approach, the image is divided to estimate the average power spectrum [2, p.142]. In the Kalman filtering approach, the image is di-

vided into sections or strips to ease the computational load and complexity by reducing the matrix size [9, p.327],[44,55]. Hunt and Trussell [45] proposed a locally adaptive image processing method by sectioning the image and applying a modified MAP restoration algorithm. Here the sectioning is equivalent to the decomposition of the filtering process into localized convolutions.

Rajala and Figueiredo [35] are the first researchers who have actually incorporated the segmentation concept into an image restoration method, realizing that the usual assumption of a single characterization for the whole image is not correct. They segment the image into regions by thresholding the masking function [34,56] which is the measure of spatial activity. The reasoning behind the segmentation is to adjust the parameters of the difference equation for each of the homogeneous regions. Jinchi et al. in their recently reported work [57] also use the masking function to segment the image. Again, the segmentation concept is used to accommodate the differences of model parameters for different regions. We would like to point out that in all of the above a single image restoration technique for the whole image is used.

Though it is in primitive form, the paper by Qian et. al [58] on image enhancement has the flavor of artificial intelligence. The image is segmented into regions and four different filters are used for regions with different local activities. This paper is considered to be closest to our research.

The goal of this research is to derive an automatic image restoration method which gives the best result in both the quantitative and qualitative sense. It is attempted by building a segmentation-oriented rule-based expert system with the

following major procedures: 1) Get a priori information either from the user or by computation, 2) Segment the image into several homogeneous regions, 3) Select the most suitable image restoration technique for each segmented region with the help of the knowledge base and the inference engine, 4) Apply the selected method to the corresponding regions, 5) Determine boundary region treatment, and, if desired, compute the performance criteria.

Two image segmentation methods [28,56], which are applicable to most image models, are installed in the system. The unified approach [28,29] is good for images with a relatively small number of regions, and the masking function approach [34,56] is good for images with many details.

Although a number of interesting methods for image restoration have been proposed, only a fraction of these are of practical use. About six restoration techniques are selected and installed into the system, along with programs to extract the a posteriori information. The schematic diagram of the proposed system is provided in Figure 6.

4.2 Selection of Methods

We need to select several image restoration techniques, and in fact we implement about 6 methods. Some procedures are designed for a very general problem. Few assumptions are made about the type of image to be recovered and these methods require little a priori knowledge. Other methods are designed to

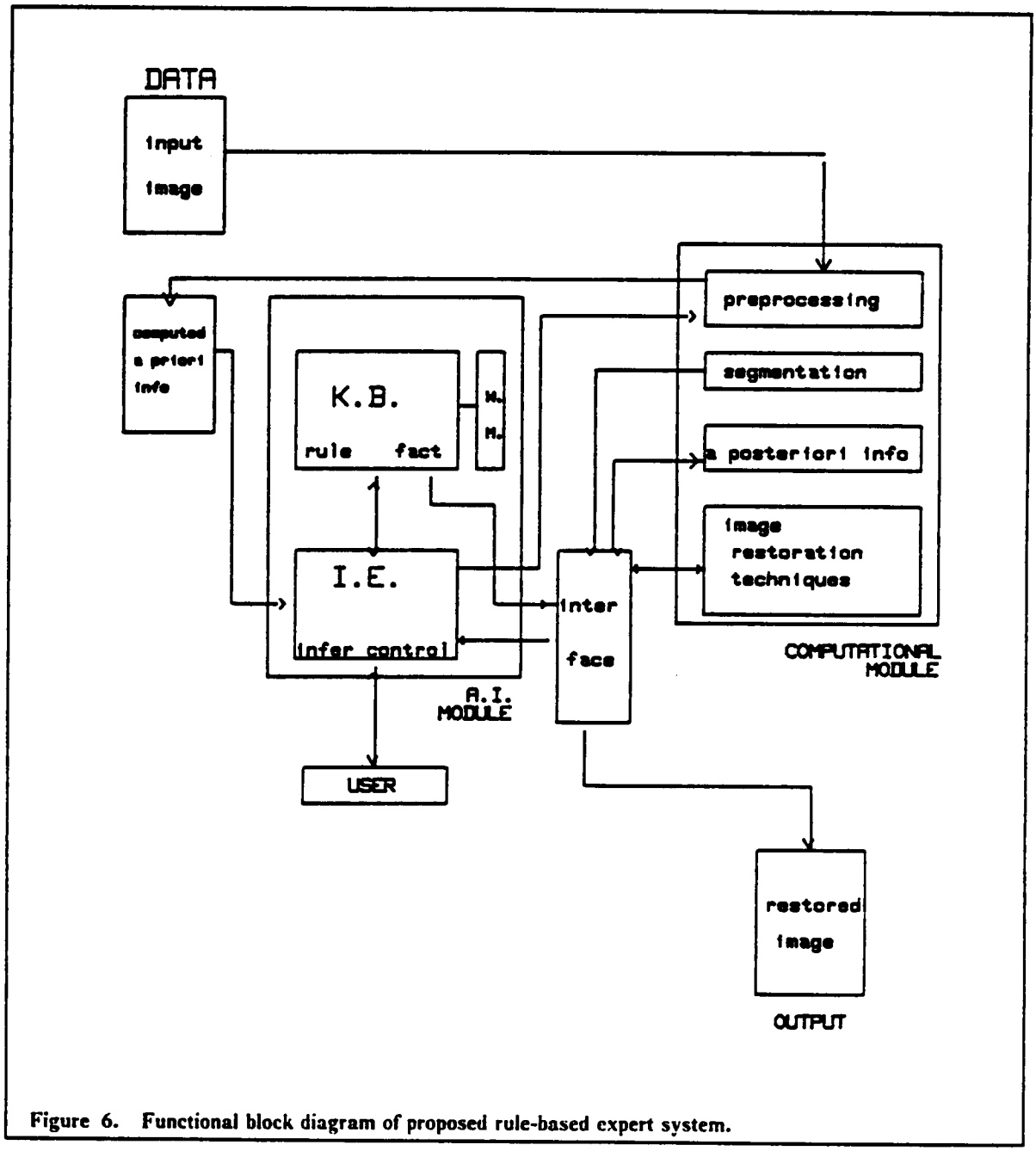

Figure 6. Functional block diagram of proposed rule-based expert system.

treat a very specific case. Such methods use a great deal of a priori knowledge. The important selection criterion is the ability to solve realistic problems. According to Hunt [3], realism in the application of an image restoration may be measured by the following aspects:

1) an image restoration technique should be computable at an average computer facility,
2) the computational requirements of the restoration technique should be applicable to pictures of reasonable size,
3) a realistic image restoration technique must be successful in the presence of the information that is available a priori, or must be a technique that is relatively insensitive to errors in the state of knowledge of the a priori information.

Considering those requirements, a preliminary selection of the possible candidate techniques has been made as follows:

- constrained least squares filter
- geometric filter
- homomorphic filter
- MAP method
- maximum entropy method
- Wiener filter

The fuzzy set method is a powerful tool, but since the computational load is too big, we dropped it from the list. With the selected methods above, most of re-

ported restoration methods can be deduced by adjusting parameters or constraint matrices.

Other software that was implemented consists of segmentation algorithms and a posteriori information computation algorithms.

The interface module controls the order of processing for each of the segmented regions. Computed a posteriori information is transferred to the A.I. module to help in selecting the correct restoration method. Section 4.6 gives more details.

4.3 Generalized Masking Function

It is generally known that at sharp transitions in image intensity the contrast sensitivity of the human visual system decreases with the sharpness of the transition and increases approximately exponentially within limits as a function of spatial distance from the transition [116].

With this property in mind, Anderson and Netravali [34] define the masking function M_{ij} at coordinate i,j as a measure of spatial detail to be

$$M_{ij} = \sum_{p=i-k}^{i+k} \sum_{q=j-l}^{j+l} C^{\|(i,j)-(p,q)\|} [|m_{pq}^{H}| + |m_{pq}^{V}|] \qquad (33)$$

where $\|(i,j) - (p,q)\|$ denotes the Euclidian distance between positions (i,j) and (p,q); m_{pq}^{V} and m_{pq}^{H} are the vertical and horizontal slopes of the image intensity at

(p,q) respectively; C is a constant controlling the rate of exponential decay of the effect of an image intensity transition on its neighbors; and k, l are constants controlling the size of the relevant neighborhood around (i,j).

It is clear that M_{ij} increases monotonically with the amount of spatial detail in a two-dimensional neighborhood surrounding a picture element. Rajala and Figueiredo [35] show that the masking function approach works well with C = .35, k = l = 1. Their test image was the face of a girl. They derive m_{pq}^{V} and m_{pq}^{H} by

$$m_{pq}^{V} = \frac{1}{v_1} \sum_{u=p}^{p+v_1} g(u,q) - \frac{1}{v_2} \sum_{u=p-v_2}^{p} g(u,q) \tag{34}$$

$$m_{pq}^{H} = \frac{1}{w_1} \sum_{u=q}^{q+w_1} g(p,u) - \frac{1}{w_2} \sum_{u=q-w_2}^{q} g(p,u) \tag{35}$$

A thresholding operation is used to segment the range of values of the measure of spatial activity M_{ij}, such that the image will be divided into regions Ω_p, $p = 1,2,...,k$. The region Ω_p is chosen if

$$a_{p-1} < M_{ij} < a_p \tag{36}$$

where a_p is chosen subjectively depending on the range of M_{ij} and the number of regions desired. Equations (34), (35) look reasonable, but they turn out to be unable to handle many situations, especially noisy images. It also generates unusually high values around the edges, even when v_i and w_i are set to 3. To take care of this deficiency, we modified equations (34) and (35) as

$$m_{pq}^{V} = \frac{1}{v_1 + 1} \sum_{u=p}^{p+v_1} \sum_{v=q-1}^{q+1} g(u,v) - \frac{1}{v_2 + 1} \sum_{u=p-v_2}^{p} \sum_{v=q-1}^{q+1} g(u,v) \qquad (37)$$

$$m_{pq}^{H} = \frac{1}{w_1 + 1} \sum_{u=q}^{q+w_1} \sum_{v=p-1}^{p+1} g(v,u) - \frac{1}{w_2 + 1} \sum_{u=q-w_2}^{q} \sum_{v=p-1}^{p+1} g(v,u) \qquad (38)$$

Equations (37) and (38) are better able to cope with noisy situations and do not generate unusually high values. A result of the application of the modified masking function approach is shown in Figure 7 along with the original. As seen in Figure 7, there are some isolated edges and disconnected boundaries. To resolve this problem, we introduce the direction information of the slope into the segmentation process. We define that an edge pixel, with coordinate (x_1, y_1) in the predefined neighborhood of (x,y), has an angle similar to the pixel at (x,y) if

$$|\alpha(x,y) - \alpha(x_1, y_1)| < A \qquad (39)$$

where A is an angle threshold. $\alpha(x,y)$ is decided by the ratio between horizontal and vertical slopes at (x,y) according to $\alpha(x,y) = arctan(m_{xy}^{H} / m_{xy}^{V})$. We refer to Equations (37),(38), and (39), together with (33), as the generalized masking function approach. The result of applying this generalized masking function approach, to the same original that generated the previous result, is given in Figure 8. We set v_i and w_i as 2, and A as 15 degrees. As seen in Figures 8, the isolated small regions have been absorbed and boundaries are widened and connected.

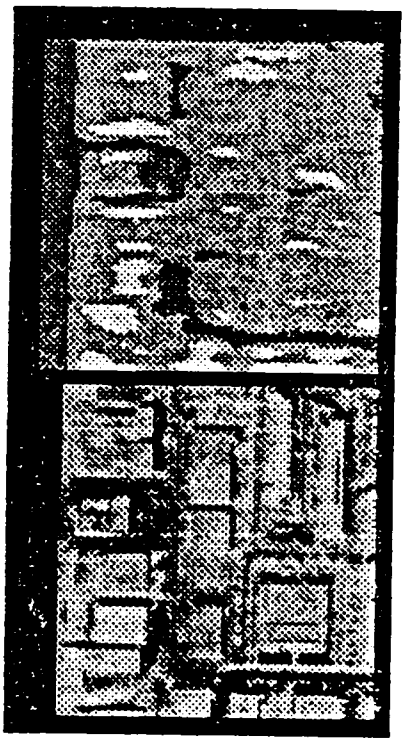

Figure 7. A result from applying the modified masking function approach.

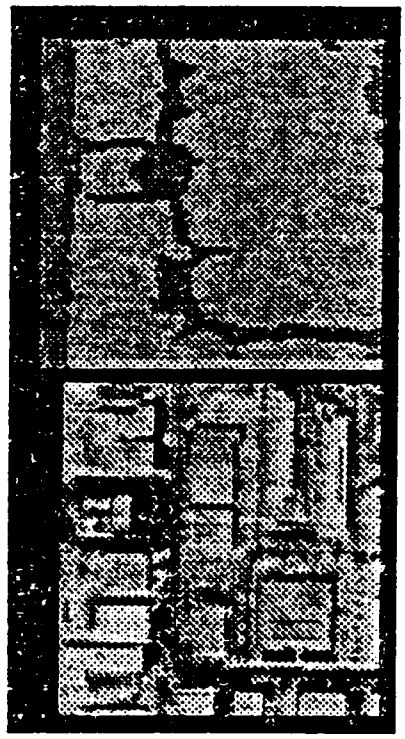

Figure 8. A result from applying the generalized masking function approach.

4.4 Point Spread Function Estimation

We may often assume that the point spread function (PSF) is known. Yet many situations arise, in which it is not known, and must be estimated. We suggest and implement two methods of identifying the PSF, that have been applied successfully, including in the present research application.

4.4.1 Zero Recognition Approach

The zero recognition approach can sometimes serve as a convenient technique for estimating the detailed form of h(x), provided enough of the zeros of the optical transfer function (OTF) can be recognized. When the form of the PSF is simple, the OTF tends to possess pronounced real zeros, which can be readily recognized in the spectrum of a recorded blurred image. Figures 9, 10, and 11 show the Fourier magnitude spectrum of some typical point spread functions; linear motion, defocus (square aperture), and atmospheric blur respectively. All point spread functions have been normalized. As expected, the OTF of atmospheric blur does not have zero crossings in it, which means we can not estimate the PSF in this case by the zero recognition approach.

The Fourier spectrum G(u,v) of a degraded image g(x,y), does not exhibit clear zero crossings. This is illustrated in Figure 13, which is the Fourier

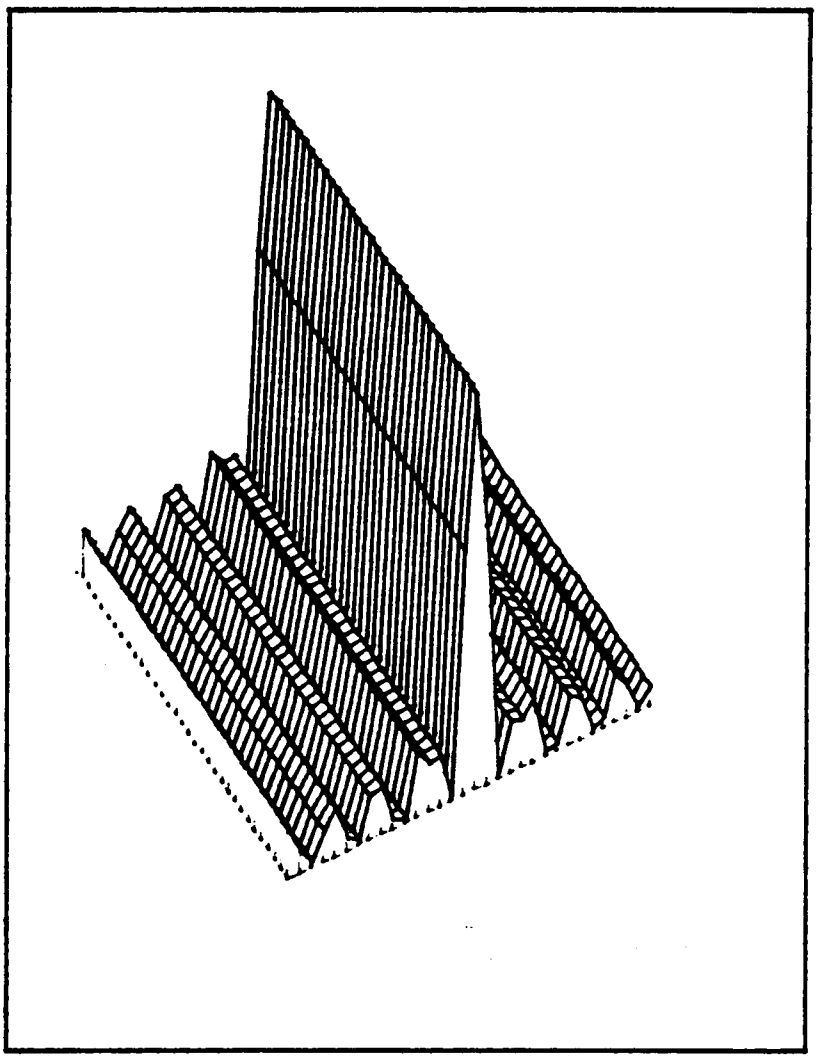

Figure 9. Fourier magnitude spectrum of linear motion blur.

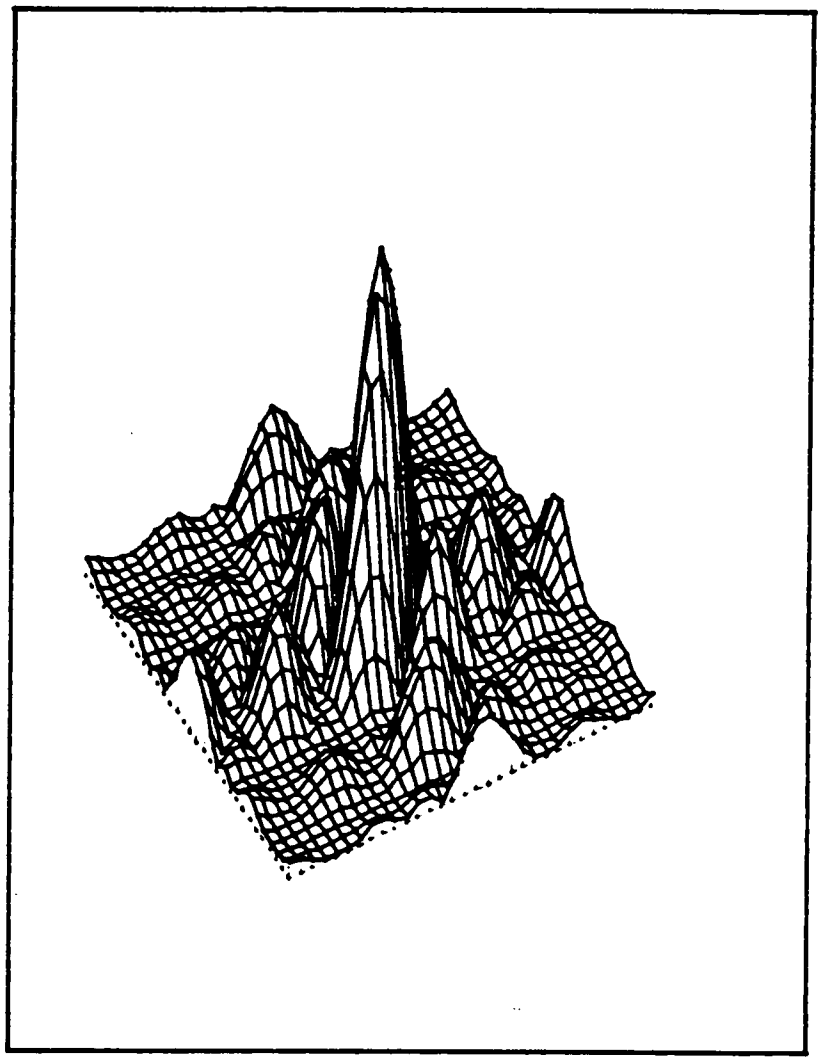

Figure 10. Fourier magnitude spectrum of out-of-focus blur (square aperture).

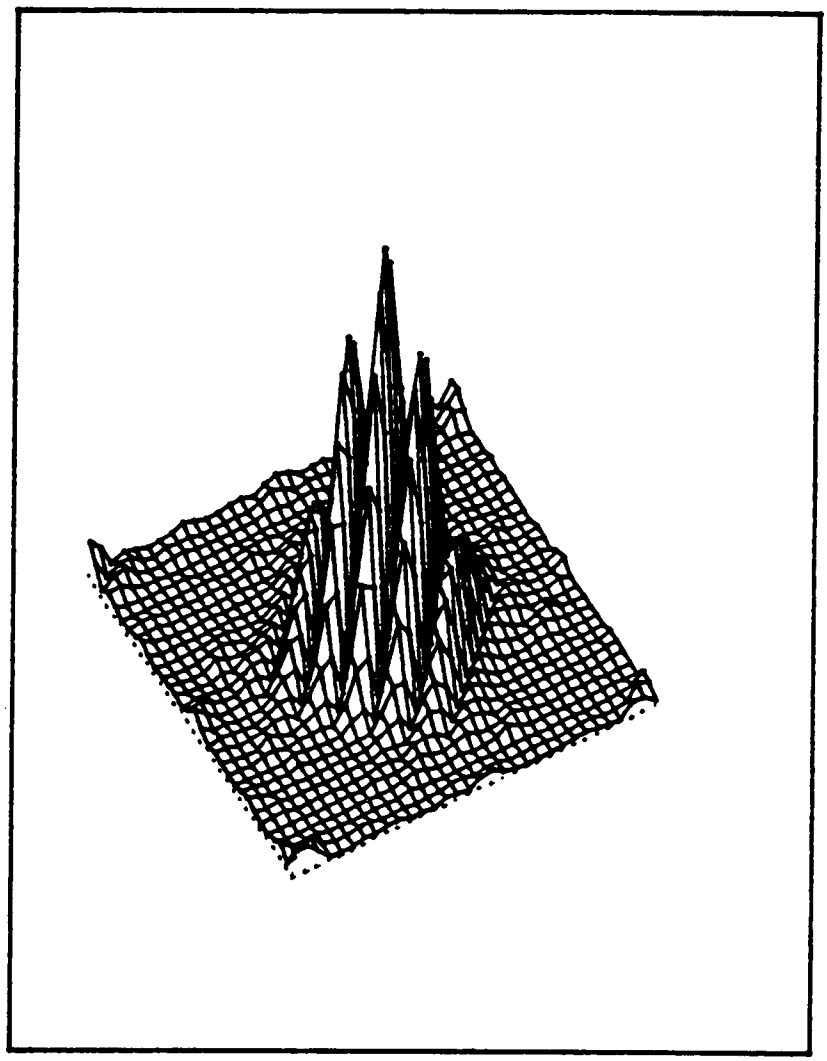

Figure 11. Fourier magnitude spectrum of atmospheric blur.

magnitude spectrum of the image degraded by the motion blur of Figure 9. The magnitude of Fourier spectrum F(u,v) of the original image f(x,y) is shown for comparison in Figure 12. To compensate for the effect of the noise, each column of G(u,v) is averaged. Subsequently the zero crossings are detected to determine the extent of the motion blur or the radius of the aperture. The Fourier spectrum of the estimated PSF is shown in Figure 14. When we compare the result with the ideal in Figure 10, we see the resemblance between the two, except that the power is more concentrated in the main lobe for Figure 14.

4.4.2 Line Spread Function Approach

The other method we implemented, to estimate the PSF, is by analysis of lines in the image. An image often possesses structures that can be identified as unresolved edges, that is, edges whose size is unresolved within the spatial extent of the PSF of the image formation system [3,97]. Analysis of the images formed by such lines produces direct information about the PSF. An additional assumption is required, such as rotational symmetry, to recover the PSF from the line spread image.

The simplest case is that of a boundary, between two different intensity levels, that extends in a north-south direction. This corresponds to an underlying functional form of a step discontinuity. We get this kind of scene structure from the checkerboard image which will be shown in a later chapter.

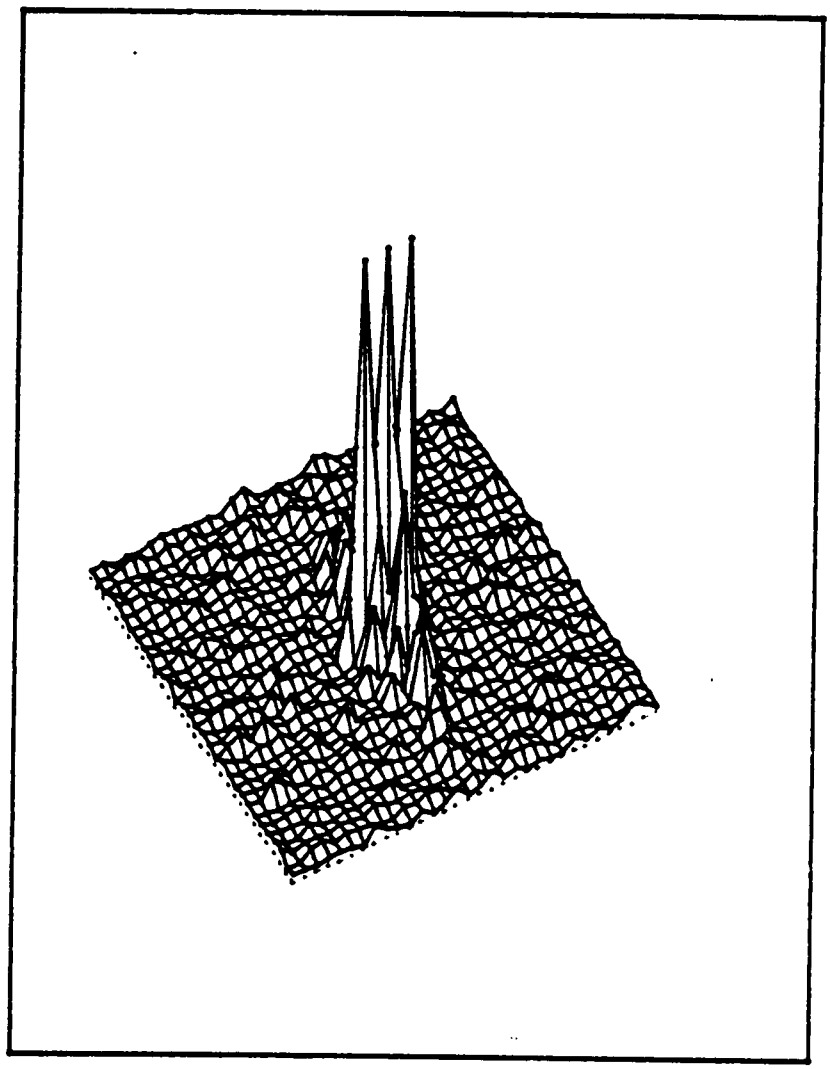

Figure 12. Fourier magnitude spectrum of original image.

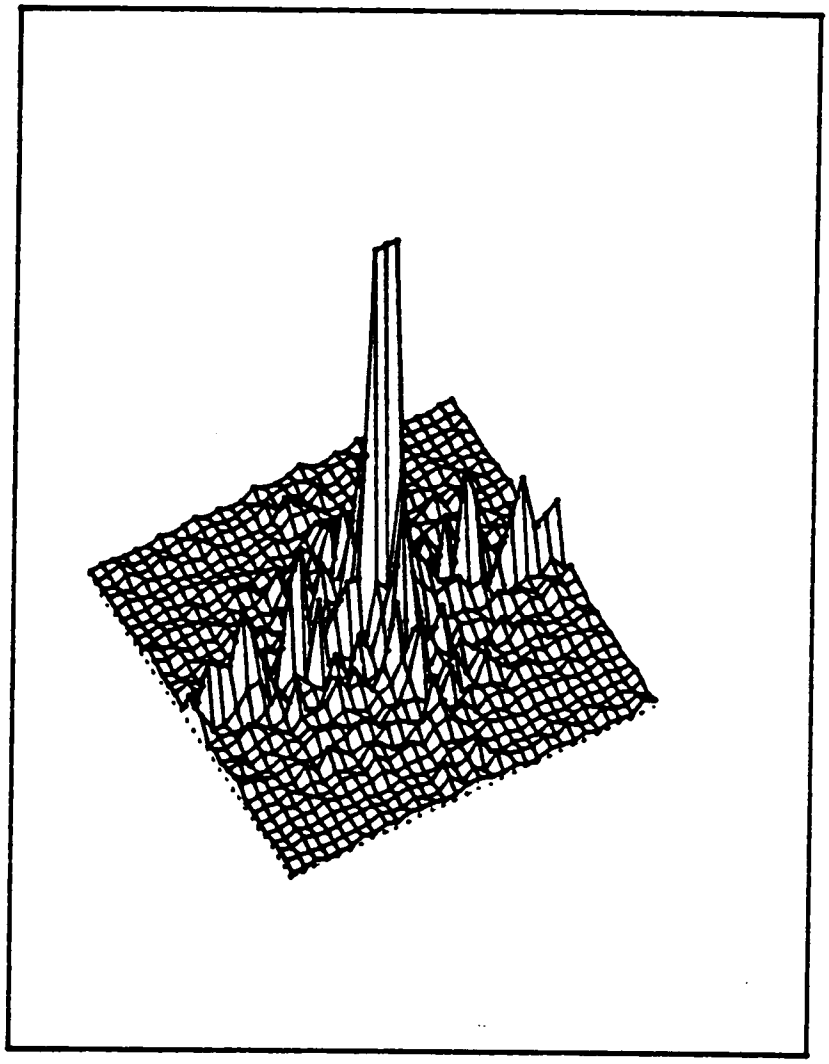

Figure 13. Fourier magnitude spectrum of motion blurred image.

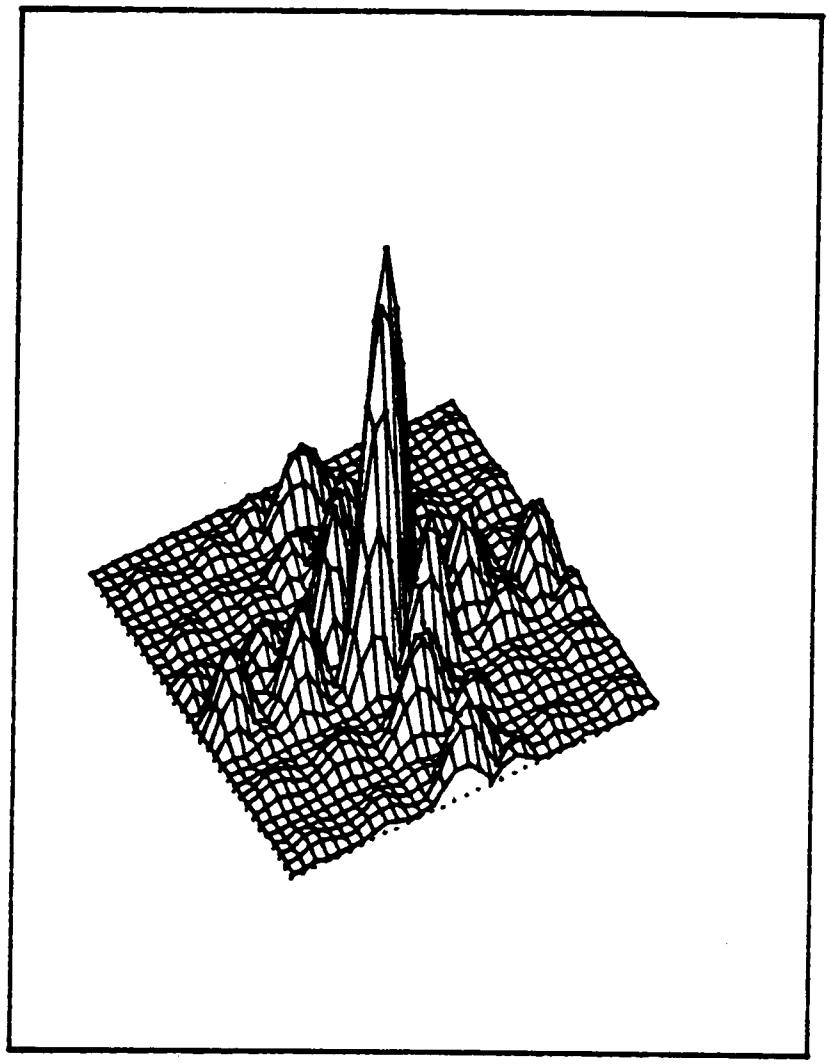

Figure 14. Fourier magnitude spectrum of PSF estimated by zero recognition (cf. Figure 10).

Take a 14-by-14 section from the image which centers on the boundary. The least-squares straightline approximation to the pixel values is computed for each row. The rearranging of this line defines a temporary origin for each row. We average over the columns 4 pixels to the left of this origin to 4 pixels to the right of this origin, and the result of this averaging is approximated using a cubic spline method, which results in a 9 point PSF estimate.

Two examples using this approach are given in Figures 15 and 16. The line spread function (LSF) approach is more powerful than the zero recognition approach if the subject image has a clear line in it. The zero recognition approach is unable to estimate the atmospheric blur because there are no zero crossings in the spectrum of such blur. On the other hand, the zero recognition approach does not require a clear line in the subject image in order to estimate the blur parameters.

4.5 Rule-Based Knowledge System

We represent knowledge by logic expressions. Logic formulations represent knowledge in a manner different from other commonly used approaches, such as semantic networks or O-A-V triplets [15]. Ordinarily, when representing facts, this is done because we want to retrieve these facts directly. They may be the values associated with an object or an attribute. Ordinarily we search to locate the needed values. Logic is a bit different. If we assert a fact in predicate calculus, which is a common logic system, its value must be either true or false. For

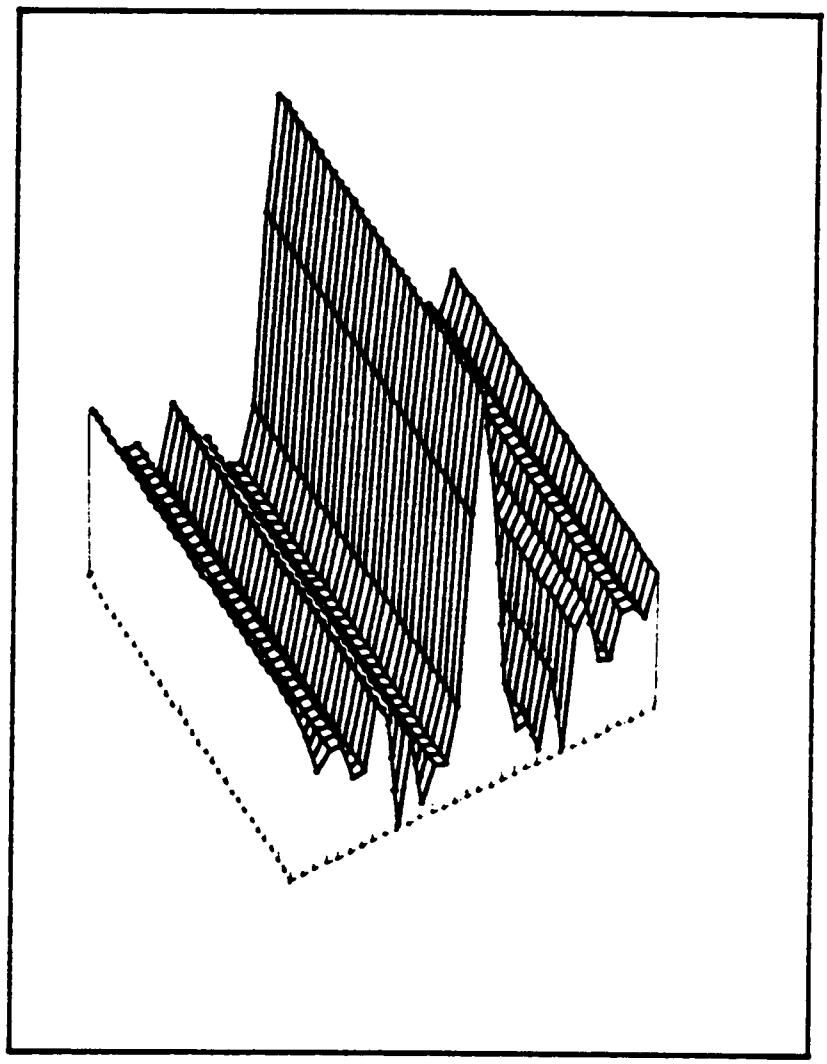

Figure 15. PSF estimation of motion blurred image by LSF approach (cf. Figure 9).

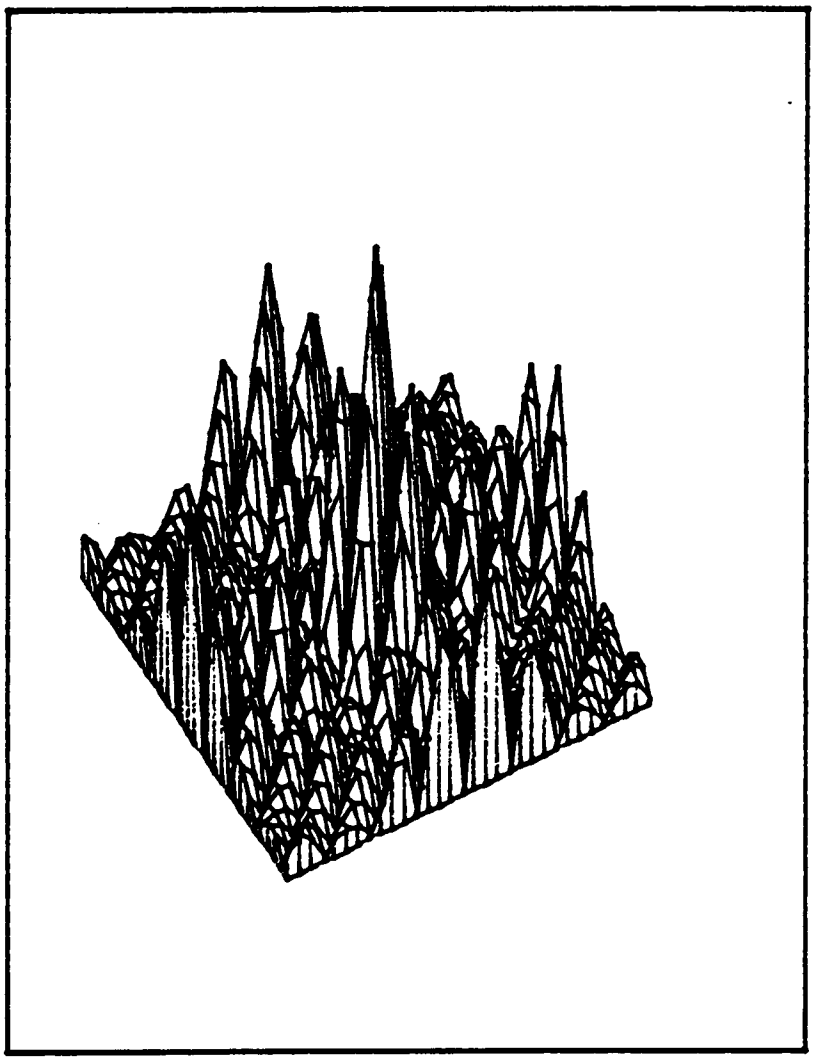

Figure 16. PSF estimation of atmospheric blurred image by LSF approach (cf. Figure 11).

example, a simple fact such as a medium signal-to-noise ratio (MSNR) can be expressed by

$$MSNR = SNR \ .GE. \ 10 \ .AND. \ SNR \ .LE. \ 20 \tag{40}$$

Only if both conditions on the right side are met, does the logical value of MSNR become true.

The control strategy of the inference engine is a combination of backward and forward chaining. The premises of the rules are examined to see whether or not they are true, given the information on hand. If so, then the conclusions are added to the list of facts known to be true. Eq. (40) is an example of forward chaining inference. Backward chaining takes control of the inference engine next. The rule has the following format:

CONDITION .AND. ... .AND. CONDITION ACTION

The left-hand side is composed of a set of CONDITIONS which are evaluated on the data in backward fashion. Backward chaining systems are also called goal-directed systems. Here ACTION can be regarded as a goal statement. For example,

$$LSNR \ .AND. \ PSF \ .AND. \ FAST \quad USE-INVERSE-FILTER \tag{41}$$

where LSNR refers to large signal-to-noise ratio, PSF means that a PSF is available, and FAST means that a fast result is requested.

The system holds about 16 prompts for getting information from the user, and 25 facts and rules. As stated before, we use the logical system to represent the knowledge base.

Considering the fact that the present expert system needs a lot of computational modules in it, we are inclined to use the FORTRAN language. FORTRAN supports such data types as LOGICAL and CHARACTERS. Those features are used exclusively in the A.I. module of the system. Our knowledge system is a bit different from the ordinary common expert systems in the sense that it contains a relatively large computational module. The A.I. module is small compared to the computational module. The Litho system [117] developed at Schlumberger for petroleum exploration in 1982 has structures similar to the present one.

4.6 Implementation

4.6.1 Functional Description

Our system consists of one main program, 11 major subroutines, and numerous minor subroutines, such as FFFT, IFFT, INDAT etc. The major subprograms are the following:

MASK: segment by the masking function approach,

SEGMENT: segment by the unified approach,

POSTERI: get a posteriori information from the image,

EXPERT: decide proper image restoration scheme by a rule-based knowledge system,

CNSTR: restore by constrained method,

GEOMET: restore by geometric filter,

HOMO: restore by homomorphic filter,

MAP: restore by maximum a posteriori method,

MAXENT: restore by maximum entropy method,

WIENER: restore by Wiener filter,

PERFORM: compute the performance criteria.

The program flow chart is given in Figure 17. In most cases, major subroutines can be bypassed by users if they choose such option. This option is added to the system as a tool to compare the performance with the traditional methods. First, the subject image is read into the system. The image is then segmented by either the masking function or the unified approach. If we want to process the whole image at once, we may by-pass this step. Subsequently, the interface module takes control. It selects one region to be processed. The selected region is sent to POSTERI to derive a posteriori information such as the PSF. Now the subject region is passed on to the EXPERT module where one or two restoration methods are recommended. One of the restoration methods is activated. After all of the segmented regions have been processed, we have restored the degraded image. Finally, the performance criteria are computed. A typical example of an interactive terminal session is provided in Appendix A.

4.6.2 Modularity of the System

Another aspect of the proposed system is its modularity. Each major part of the system is inter-related only by the interface module. Each module, such as the A.I. module or the computational module, can be expanded or modified independently without affecting other parts of the system. Expansion or upgrading of the system can be done easily when new approaches are introduced or developed.

Each restoration method can be regarded as a filter, whether in closed form or not. Iterative methods, such as the MAP method, can not be expressed in a closed form. We may express these filters in a parametric form as follows

$$H(\omega) = H(\omega; f,g,n,SNR,PSF,K)$$

where ω represents frequency and f, g, and n represent original, degraded image, and noise process respectively. K denotes all necessary constants. Most computations are done in the frequency domain to make use of the FFT algorithm. For each different image, degradation, noise, and PSF, the filter uses different parameters. The implementation details for each of these filters are given in Section 6.3. If exact information is not available, it is estimated from the degraded image itself.

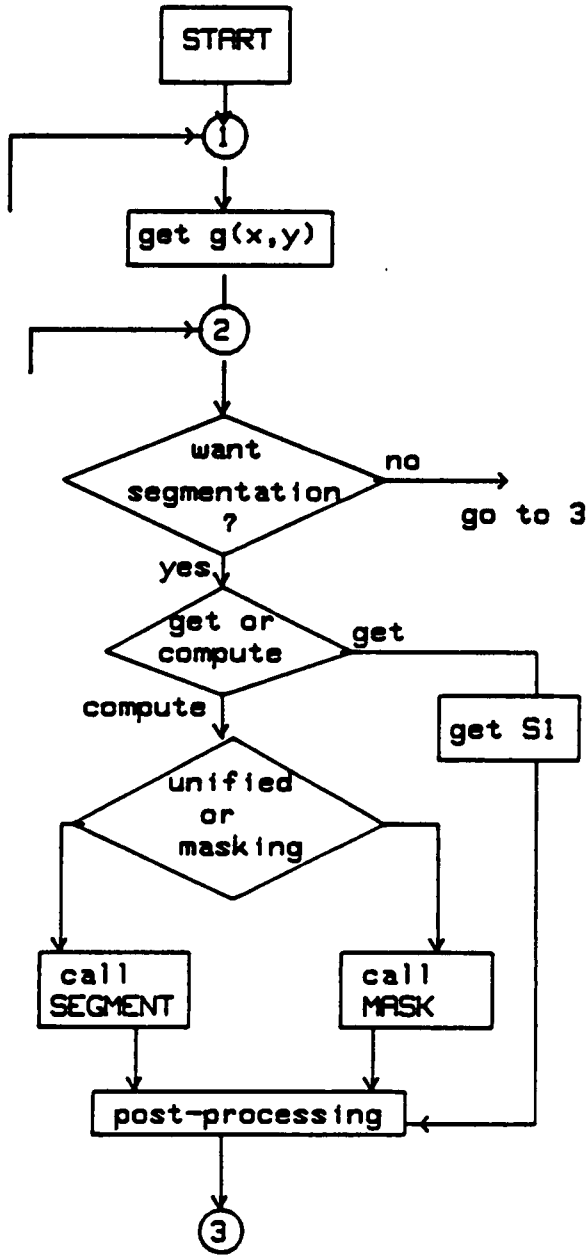

Figure 17. Simplified program flow chart.

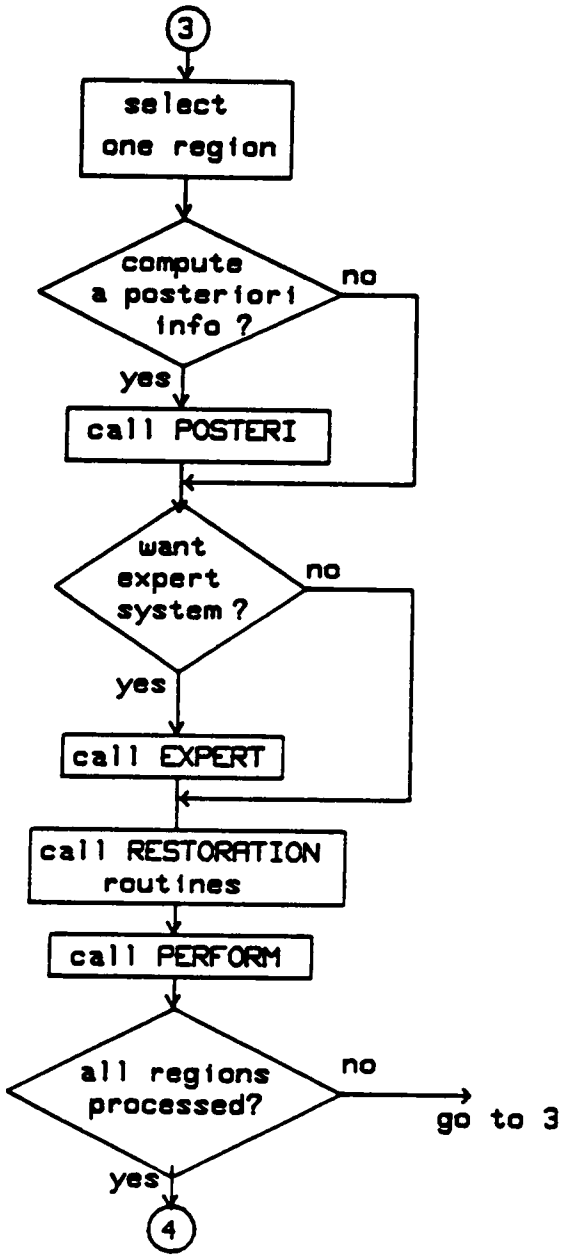

Figure 17. Continued

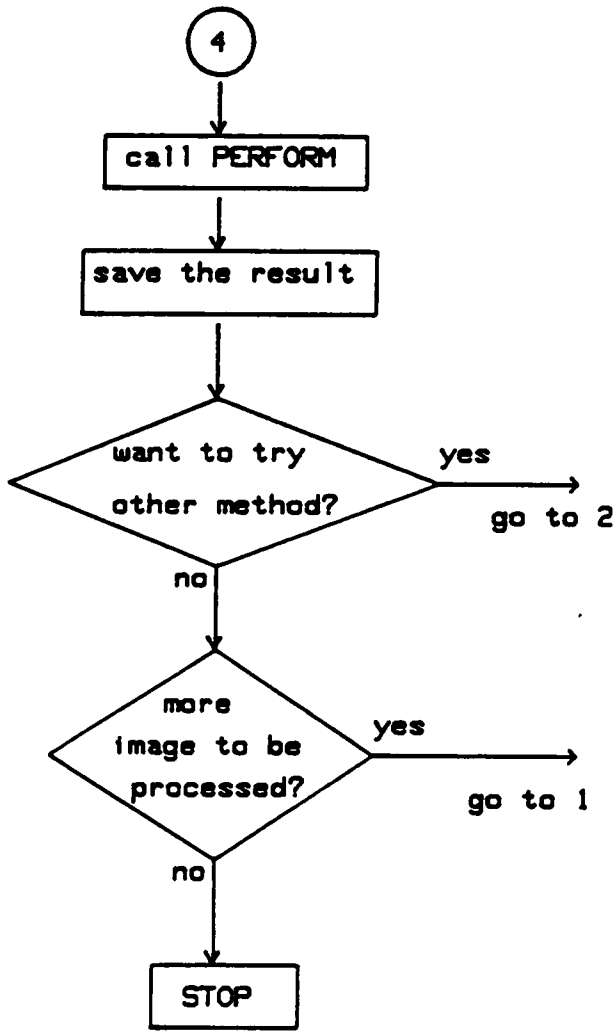

Figure 17. Continued

Chapter V. Performance Criteria

There are two aspects to assessing the performance of an image restoration method: quantitative and qualitative measures. As a quantitative measure, the MSE criterion is most widely used. The MSE criterion weighs all errors equally, regardless of their location in the image. For a qualitative measure, a large number of individuals needs to assess quality somehow. The underlying criterion can be approximated with a quantitative measure, and several of these so-called qualitative performance criteria have been proposed. These measures range from simple, and mathematically tractable measures, to measures based on complex models of the human visual system.

5.1 Quantitative Image Quality Measures

The most commonly used measure of image quality is the mean square error (MSE) criterion. The MSE for a digital image or image segment is defined by

$$MSE = \frac{1}{N_f} \sum_k (f_k - \hat{f}_k)^2 \tag{42}$$

where f and $\hat{f}$ represent the original and the restored image respectively, $\sum_k$ represents a 2-D summation over all pixels in the image or image segment, and N_f denotes the number of pixels it consists of. A measure based on the absolute value of the difference is called the mean absolute error (MAE) criterion. MAE is defined by

$$MAE = \frac{1}{N_f} \sum_k |f_k - \hat{f}_k| \tag{43}$$

MSE and MAE can be normalized with respect to the measure associated with the original image. The normalized mean square error (NMSE) and normalized mean absolute error (NMAE) are given by the following equations [118].

$$NMSE = \frac{\sum_k (f_k - \hat{f}_k)^2}{\sum_k f_k^2} \tag{44}$$

$$NMAE = \frac{\sum_k |f_k - \hat{f}_k|}{\sum_k |f_k|} \tag{45}$$

It is also meaningful to define measures based on the signal-to-noise ratio (SNR). Root-mean-square SNR (RMSSNR) and absolute SNR (ABSSNR) are defined as follows [5]

$$RMSSNR = 10\, log_{10} \frac{\sum_k f_k^2}{\sum_k (f_k - \hat{f}_k)^2} \tag{46}$$

$$ABSSNR = 20\, log_{10} \frac{\sum_k |f_k|}{\sum_k |f_k - \hat{f}_k|} \tag{47}$$

5.2 Qualitative Image Quality Measures

The measures described in the previous section are simple in nature and can be computed rather easily. They do however, not correlate well with subjective quality evaluations. A number of measures designed to improve this shortcoming have been reported [7, 12, 115]. It is known that the response of the human visual system to input light intensity is nonlinear, and this nonlinearity is often modelled as a logarithmic function. Logarithmic mean square error (LOGMSE) [7] takes into account this nonlinearity.

$$LOGMSE = \frac{\sum_k [\log_{10}(1 + f_k) - \log_{10}(1 + \hat{f}_k)]^2}{\sum_k [\log_{10}(1 + f_k)]^2} \tag{48}$$

Laplacian mean square error (LMSE) is a measure that takes into account the importance, to the human observer, of edges. LMSE is defined by

$$LMSE = \frac{\sum_k (G_k - \hat{G}_k)^2}{\sum_k G_k^2} \tag{49}$$

where

$$G_{ij} = f_{i+1j} + f_{i-1j} + f_{ij+1} + f_{ij-1} - 4f_{ij}, \tag{50}$$

and $\hat{G}$ is defined similarly on the basis of $\hat{f}$. Note that the support of G is the interior of the support of f, since G is computed from the nearest neighbors. The gradient mean square error (GMSE) criterion [12] is obtained by defining G_{ij} in Equation (49) as,

$$\begin{aligned} G_{ij} = |&f_{i+1j-1} + 2f_{i+1j} + f_{i+1j+1} - f_{i-1j-1} - 2f_{i-1j} - f_{i-1j+1}| \\ + |&f_{i-1j+1} + 2f_{ij+1} + f_{i+1j+1} - f_{i-1j-1} - 2f_{ij-1} - f_{i+1j-1}| \end{aligned} \tag{51}$$

$\hat{G}$ is defined similarly, based on $\hat{f}$. These measures have been experimentally found to exhibit correlation with subjective evaluations that is better than those presented in the previous section. Quantitatively good images of a poor subjective quality often rate high on the above semi-qualitative measures [5]. It should be emphasized that a generally agreed-upon quantitative measure of image quality has not been discovered yet.

The wide range of situations in which image quality measures are applied makes it inappropriate to label a particular measure as best for all different kinds of applications. Instead of selecting any single criterion as our choice for measuring quality, we show and compare the values of several different measures in the experiments of Chapter VI.

Chapter VI. Experiments

6.1 Synthesis of Degraded Images

The degraded image g(x, y), is expressed by the following equation.

$$g_k = f_k * h_k + n_k \tag{52}$$

where k is a 2-D index, f_k is the original image, h_k is the PSF, and n_k is the additive noise process.

Two different originals are used here: one is a street scene taken from above and the other is a checkerboard pattern generated by computer. The size of these originals is 96 by 96.

Six different degradations have been generated. They are: motion blur (5-pixel width and 9-pixel width), defocus blur (circular and square aperture of 5-by-5 extent) and atmospheric blur (light and severe). Each PSF has been normalized. For example, the PSF of five-pixel width motion blur is represented by

$\frac{1}{5}$[1 1 1 1 1]. The PSF for defocus blur is the flat region with a constant pixel value over a specified extent. The PSF for atmospheric blur has been synthesized by $\exp(\frac{-((x-5)^2+(y-5)^2)}{\sigma^2})$, where $1 \leq x,y \leq 9$, $\sigma = 2, 4$. Noise is assumed to be white, and Gaussian, and has five different levels of variance (σ = 2, 3, 4, 5, 6).

The original images have been degraded according to Eq. (52). A few typical examples are illustrated in Figures 18 through 20. An image degraded by 9-pixel width motion blur and additive noise with variance 9 is shown in Figure 18. The original is also provided for comparison. Figure 19 illustrates out-of-focus blur with noise of variance 36. A checkerboard pattern degraded by severe atmospheric blur and noise with variance 9 is shown in Figure 20.

6.2 Generation of Test Images

The degraded images generated according to Section 6.1 can be mixed together in various ways to get more realistic situations. The result is an image that has different kinds and amounts of blur, for which segmentation into two regions looks most natural. Four examples of test images are given in Figures 21 through 24. Each figure consists of two images, the one on the top is the test image synthesized by combining two degraded images. The one on the bottom is the original undegraded image.

Figure 21 shows the combination of two degraded images: one degraded by square aperture out-of-focus blur and one degraded by 5-pixel width motion blur.

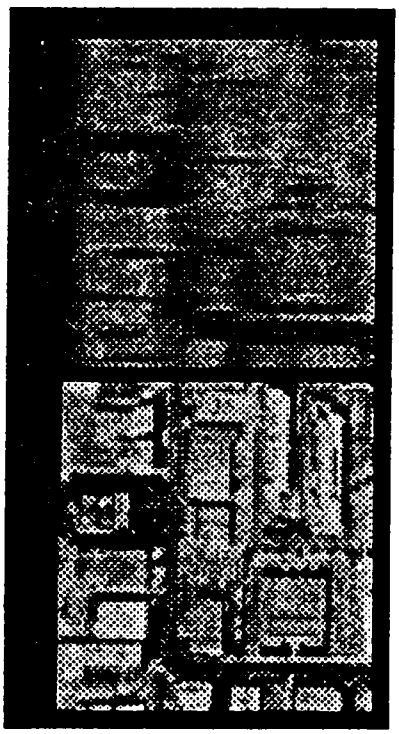

Figure 18. Illustration of degradation by motion blur and noise.

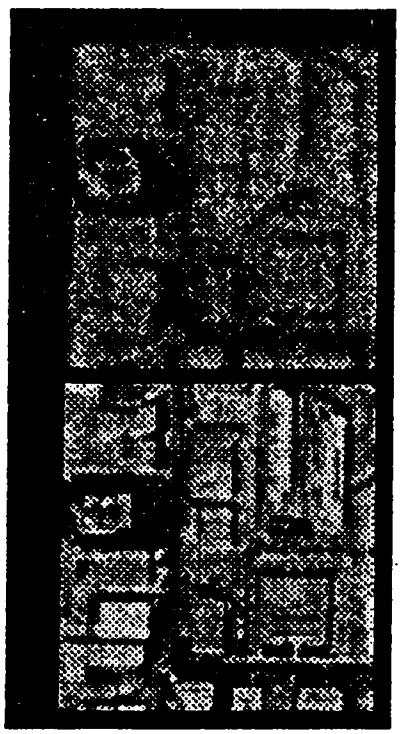

Figure 19. Illustration of degradation by defocus blur and noise.

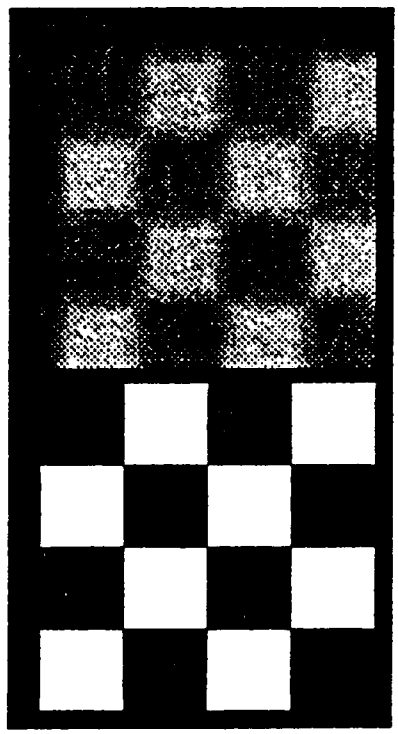

Figure 20. Illustration of degradation by atmospheric blur and noise.

In figure 22, 5-point motion blur with noise of varaince 16 and atmospheric blur with noise of variance 25 are shown in a single image. For the checkerboard image, many combinations are possible. A few of these are shown in Figures 23 and 24. In Figure 23, we illustrate motion blur in central region surrounded by a region degraded by atmospheric blur. The combination of out-of-focus blur in the background and motion blur nearby is illustrated in Figure 24. The degradation of these figures is somewhat realistic. A moving vehicle in a battle field may produce a situation similar to that of Figure 23. We may encounter this kind of degradation in everyday life. The scene of a shop display where the head of a mannequin is moving with respect to the background, also results in a situation similar to that of Figure 23. If we take a picture of a country scene from the window of a moving train, the objects in the foreground are blurred badly by a uniform camera motion blur, but the background suffers very little from this motion blur. Figure 24 represents this situation.

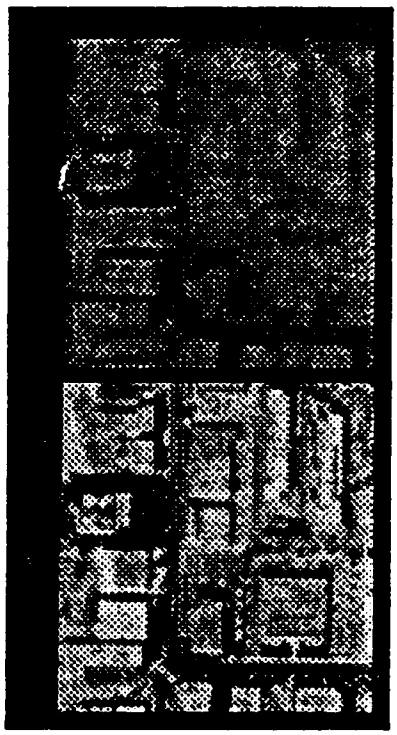

Figure 21. Test image #1: combination of motion/out-of-focus blur.

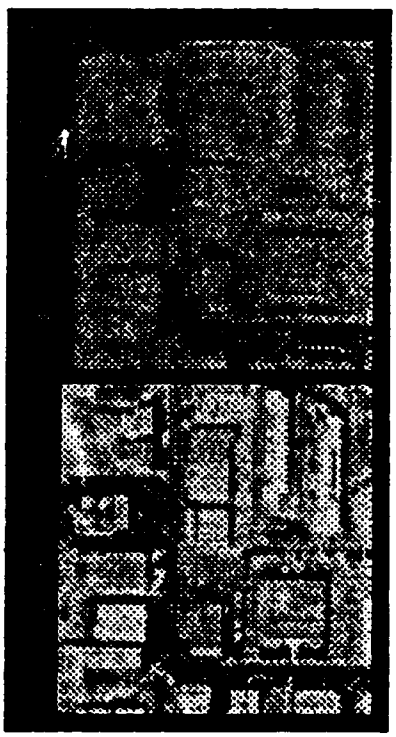

Figure 22. Test image #2: combination of atmospheric/motion blur.

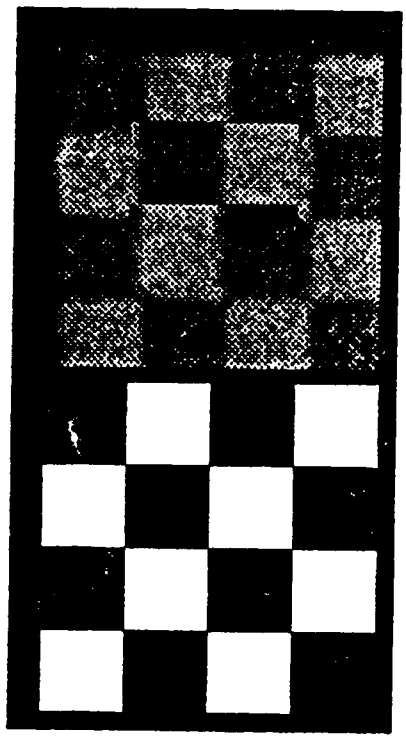

Figure 23. Test image #3: combination of motion/atmospheric blur.

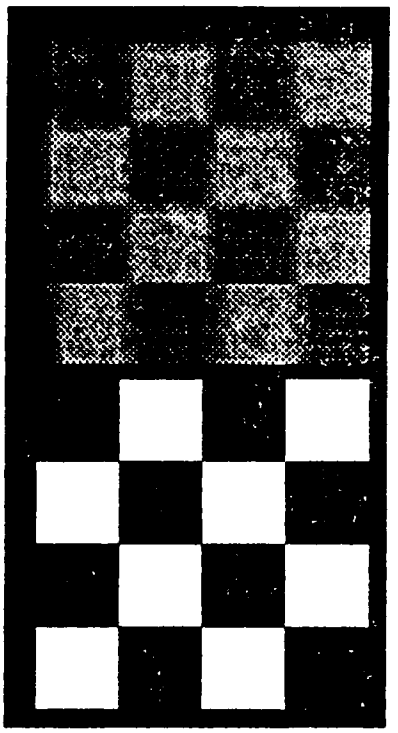

Figure 24. Test image #4: combination of out-of-focus/motion blur.

6.3 Filter Implementation

In this section, we present the implementation details of the image restoration filters installed in the system. The extent of the PSF h(x,y), is restricted to be less than 9 by 9. It is augmented with zeros to the size of 128 by 128. The degraded image g(x,y), produced by Eq. (52), is also augmented with zeros to the size of 128 by 128. The FFT of these augmented arrays, h(x,y) and g(x,y), results in H(u,v) and G(u,v) in the frequency domain. The Wiener filter (denoted by W) is implemented based on Eq. (15). Filtering is performed in the frequency domain on a point-by-point basis. The power spectrum of the original (S_f) and the noise (S_n) can be either estimated from the degraded image itself or computed exactly using the correct information. The inverse FFT of $\hat{F}(u,v)$ gives $\hat{f}(x,y)$, the restoration result, which is then limited to the extent of the image segment processed.

The homomorphic filter (denoted by H) of Eq. (17), the inverse filter (denoted by I) of Eq. (13) or Eq. (18), the geometric filter (denoted by G) of Section 2.2.2, and the linearized maximum entropy method (denoted by E) of Eq. (28), follow a procedure similar to that of the Wiener filter.

The restoration process of the constrained least-squares filter (denoted by C) of Eq. (19) is iterative. The constrained method stops iteration when the constraint, $(1. - 0.025)||n||^2 \leq ||g - H\hat{f}||^2 \leq (1. + 0.025)||n||^2$, is met. For each iteration, it increments or decrements the γ value according to a Newton-Raphson

like procedure. With an initial γ value of .01 and an initial increment of .001, convergence to the proper value of γ is usually achieved in 4-7 iterations.

The MAP (denoted by M) method is also an iterative method. The MAP method needs $\bar{f}$, the mean of the distribution of f, and $\hat{f}_0$, the initial estimate of $\hat{f}$. When exact information on f is available, f is used as $\bar{f}$. When f is not available, we use the output of the Wiener filter as $\bar{f}$. The output of the Wiener filter is also chosen as the initial estimate $\hat{f}_0$. The iteration stops when we achieve $||g - s(H\hat{f}_k)||^2 \leq ||n||^2$. The restoration by the MAP method is a slow process. Each iteration involves a lot of computation, both in time domain and frequency domain, and the convergence is slow. Trussell and Hunt [76] proposed an improved MAP method which converges faster. We implemented this new method in our system. We stop the iteration process when either the number of iterations is more than 10, or when the norm of the difference between $\hat{f}_k$ and $\hat{f}_{(k+1)}$ is smaller than 35.

6.4 Illustration of Conventional Image Restoration Approach

In this section, we illustrate the performance of various image restoration methods when they are used in a conventional way. The image restoration methods include only those which were implemented in the proposed system. Each figure contains the original image (denoted by O), the degraded image (denoted by D), and the result of six different image restoration methods (C, G, H, I, M, W). Various measures of image quality discussed in Chapter V were eval-

uated for the restored images and the results are tabulated in Tables 2 through 4.

In Figure 25, the original image is degraded by five-pixel-width motion blur with no noise added. Table 2 shows the performance criteria associated with the results in Figure 25. From the results shown in Figure 25 and Table 2, the quality of restorations appears to be good. Considering the fact that the original image in Figure 25 is not subject to any noise, the small errors in Table 2 are a natural consequence. With zero noise, it is also expected that the restoration results of the inverse filter, the geometric filter with $\gamma = 1.$ and $\alpha = .5$, and the Wiener filter are identical. As can be seen in Table 2, the error terms for the Wiener filter restoration are slightly different from those of the inverse filter. This deviation came as a result of differences in implementation details. The homomorphic filter is a magnitude-only filter that does not use any phase information. For this reason, the restoration result of the homomorphic filter suffers from a high MSE error.

Figure 26 illustrates the case where the original is degraded by moderate atmospheric blur with additive Gaussian noise of variance 25. The SNR value of this degraded image is about 15 dB. Table 3 gives the performance measures for Figure 26. Due to the large noise, the entries in Table 3 are much bigger than those of Table 2. The Wiener filter produced the best result in terms of most of the error criteria including MSE, LOGMSE, and GMSE. The restoration result from the geometric filter gave a smaller MSE than that from the homomorphic filter. Comparing the results visually as shown in Figure 26, we may rate the

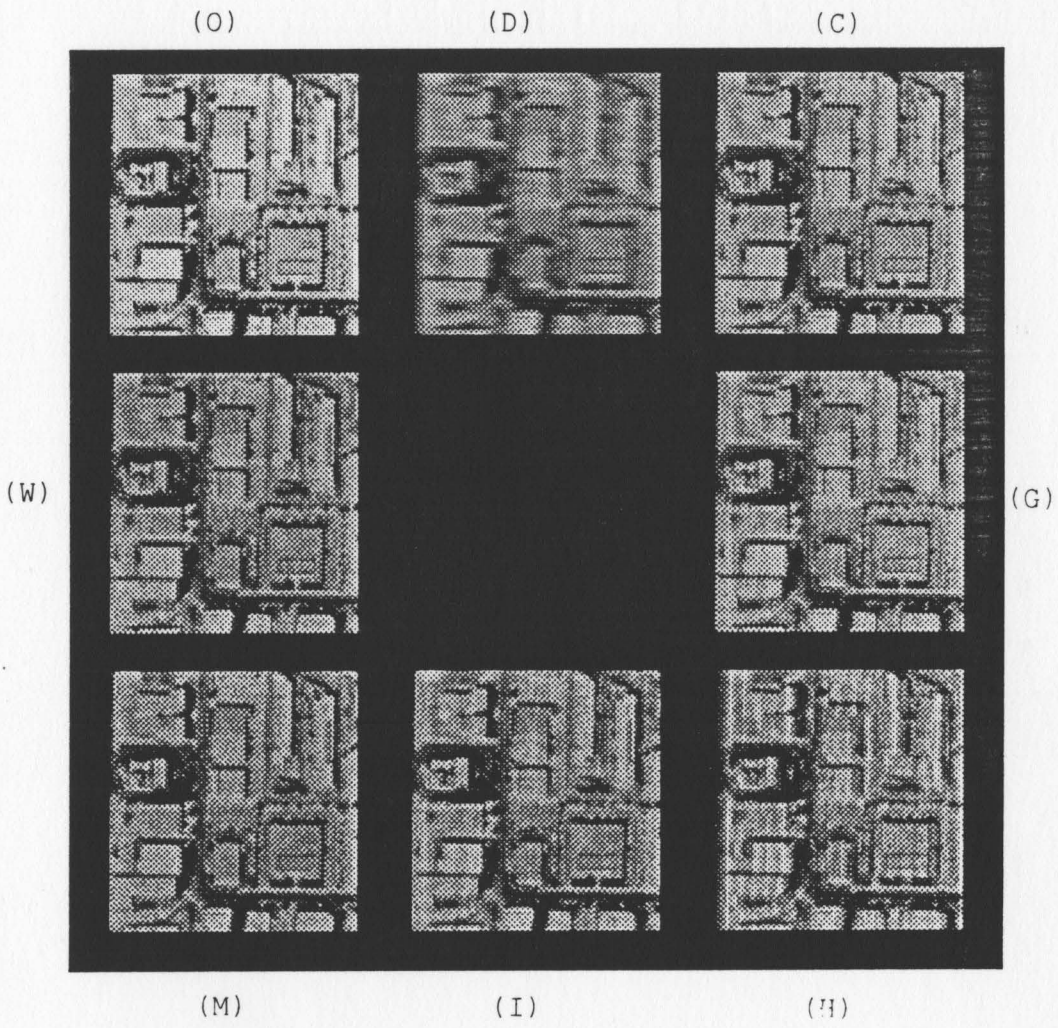

Figure 25. Illustration of restoration by conventional approach, #1.

Table 2. Performance criteria for Figure 25.

Filter Type	MSE NMAE ABSSNR	MAE LOGMSE LMSE	NMSE RMSSNR GMSE
Constrained Method	1.4326 0.0256 31.8421	0.8636 0.0013 0.0532	0.0010 30.0072 0.0064
Geometric Filter	5.8670 0.0553 25.1517	1.8657 0.0063 0.0502	0.0041 23.8843 0.0340
Homomorphic Filter	132.3172 0.2405 12.3762	8.1212 0.0441 0.8949	0.0922 10.3524 0.4312
Inverse Filter	5.8670 0.0553 25.1517	1.8657 0.0063 0.0502	0.0041 23.8843 0.0340
MAP Method	0.4940 0.0146 36.6933	0.4940 0.0002 0.0101	0.0003 34.6309 0.0009
Wiener Filter	1.5691 0.0269 31.3892	0.9098 0.0017 0.0295	0.0011 29.6119 0.0085

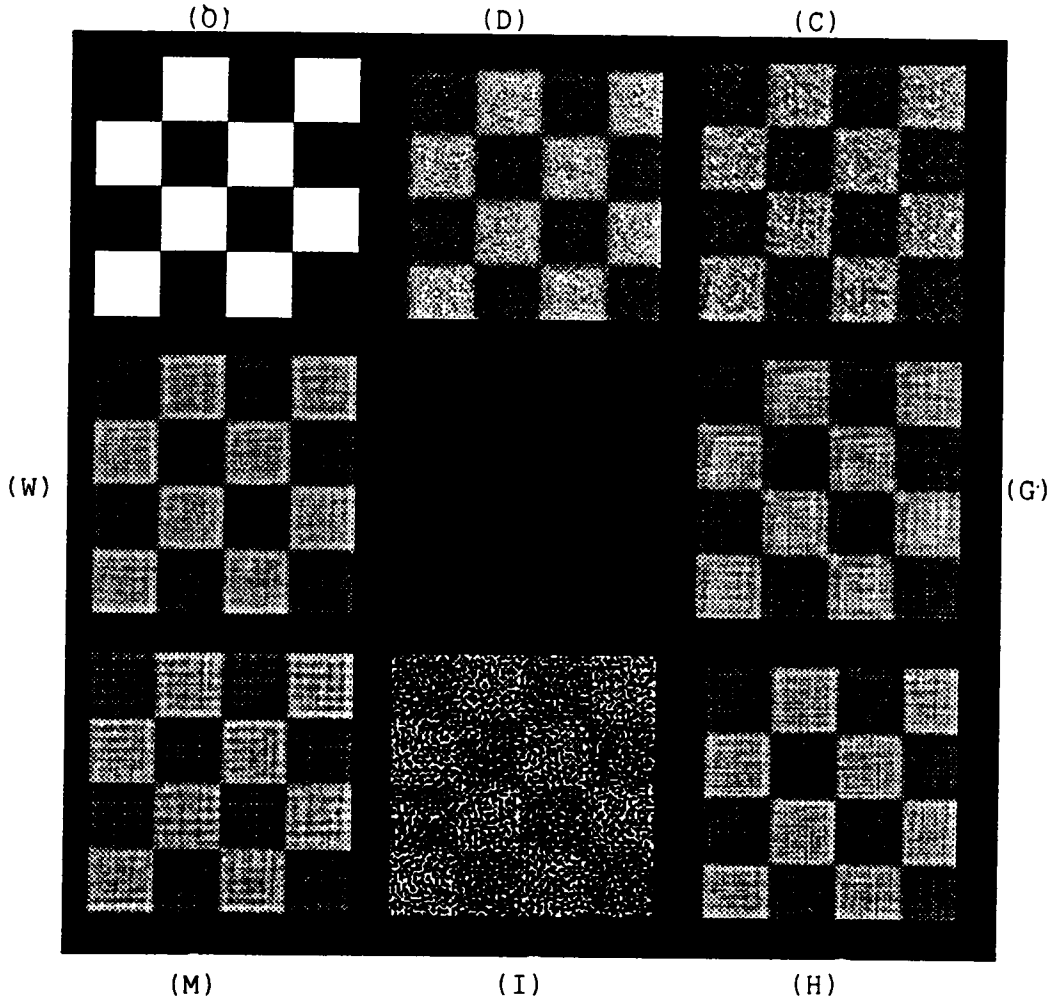

Figure 26. Illustration of restoration by conventional approach, #2.

Table 3. Performance criteria for Figure 26.

Filter Type	MSE NMAE ABSSNR	MAE LOGMSE LMSE	NMSE RMSSNR GMSE
Constrained Method	113.3175 0.1711 15.3336	8.2140 0.0087 4.6812	0.0393 14.0509 0.8562
Geometric Filter	74.4022 0.1360 17.3304	6.5270 0.0036 1.0787	0.0258 15.8780 0.5347
Homomorphic Filter	410.9936 0.3421 9.3156	16.4231 0.0324 1.6700	0.1427 8.4555 1.2416
Inverse Filter	444.6943 0.8171 1.7546	39.2203 0.2531 165.8187	0.8489 0.7160 13.0789
MAP Method	59.2540 0.1241 18.1265	5.9554 0.0043 1.0750	0.0206 16.8666 0.8617
Wiener Filter	36.4179 0.0852 21.3936	4.0884 0.0017 0.8482	0.0126 18.9807 0.3454

restoration result from the homomorphic method higher than that from the geometric filter. The computed performance given in Table 3 however, does not support this subjective observation. As discussed in Chapter V, quantitatively good images of a poor subjective quality often rate high on the semi-qualitative measures such as LOGMSE, LMSE, or GMSE. The result of the inverse filter is very poor, as expected, because of the noise amplification effect as discussed in Chapter II. The high values of LOGMSE, LMSE, and GMSE correspond to this poor appearance.

Figure 27 shows the restoration results for an image degraded by circular-aperture defocus blur and noise with variance 9. The SNR of the subject image is about 17 dB. The MAP method and the Wiener filter gave the best results both in a quantitative and a qualitative sense. The MAP filter uses the restoration result of the Wiener filter as the starting point of its iteration. The MAP filter converged at the first iteration resulting in the same restoration as the Wiener filter. The restoration result from the homomorphic filter again appears to be more pleasant than those from the constrained method or the geometric filter. The computed performance given in Table 4 however, does not support this subjective observation.

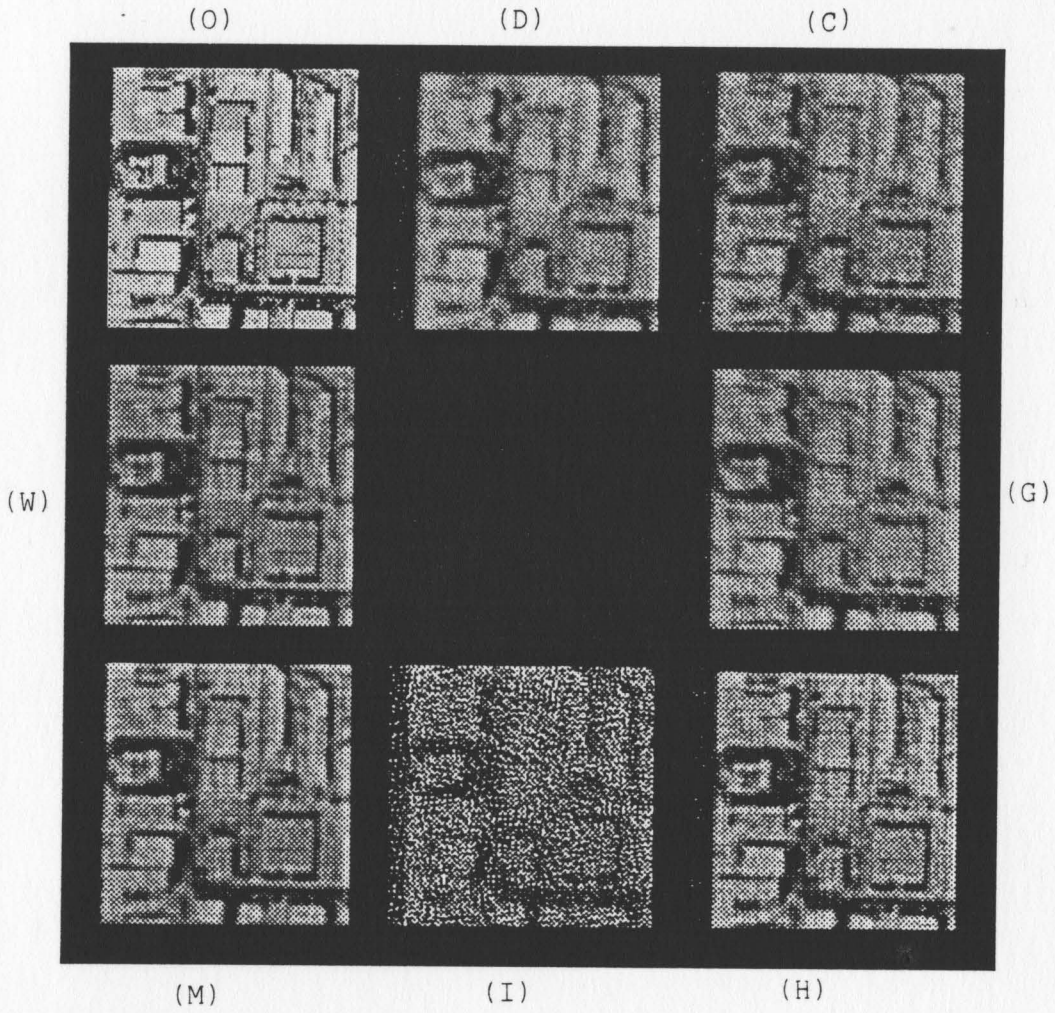

Figure 27. Illustration of restoration by conventional approach, #3.

Table 4. Performance criteria for Figure 27.

Filter Type	MSE NMAE ABSSNR	MAE LOGMSE LMSE	NMSE RMSSNR GMSE
Constrained Method	54.0371 0.1651 15.6428	5.5755 0.0261 1.8780	0.0377 14.2416 0.2424
Geometric Filter	39.3495 0.1409 17.0186	4.7588 0.0216 0.8589	0.0274 15.6192 0.2129
Homomorphic Filter	270.0096 0.3535 9.2049	11.9363 0.0935 1.9510	0.1882 7.2548 0.6904
Inverse Filter	529.3140 0.5363 5.4122	18.1059 0.1534 26.7556	0.3688 4.3315 1.5470
MAP Method	24.0712 0.1083 19.3057	3.6571 0.0138 0.6791	0.0168 17.7535 0.1209
Wiener Filter	24.0712 0.1083 19.3057	3.6571 0.0138 0.6791	0.0168 17.7535 0.1209

6.5 Image Restoration by a Segmentation-Oriented Knowledge System

The test images generated in Section 6.2 are processed by the proposed system. The restoration result and the performance criteria are illustrated in the following way. For each test image, we produce seven different results and illustrate these in two figures and one table. The first figure contains the test image (denoted by D), the restoration result by single method A, the restoration result by single method B, and the restoration result by the proposed system, using method A for one region and method B for the other region. We note that the first two restoration results correspond to those of the third generation approach discussed in Chapter III. The second figure contains the segmentation result (denoted by S) of the subject image and three residual images corresponding to the three restored images in the first figure. The table shows the performance criteria for each of the restorations. Each table has three parts: one for method A, one for method B, and one for the combined method. Each part consists of three sub-parts: one for region 1, one for region 2, and one for the whole image. The seven performance criteria discussed in Chapter V are evaluated for each of the restoration methods used.

Figure 28 shows the restoration results of a test image degraded by a combination of motion blur in the left-side region (region 1) and out-of-focus blur in the right-side region (region 2) of the image. Both regions are contaminated by additive white noise with variance 9. The segmentation result is shown in Figure 29(S). For region 1, degraded by motion blur and moderate noise, the geometric

filter (method A) is the choice of the expert system under the MSE criterion. The MAP method (method B) is selected for region 2 which suffers squared-aperture defocus blur and a moderate level of noise. The SNR values for region 1 and region 2 are 11 dB and 15 dB respectively. The MSE difference for region 1 between two methods is about 5.99. As seen in Table 5, the MAP method gives the restoration result with lower LMSE value in region 1. Lower LMSE means that the restored image has sharper edges. This can be confirmed in Figure 28(M). Other than that, the geometric filter outperforms the MAP method in all other criteria. As for region 2, the restoration result by the MAP method outperforms that for the gometric filter in terms of all the criteria. The residue image of region 2 by the MAP method, as seen in Figure 29(M), does not exhibit any trace of the original patterns. We see however a certain pattern, such as the shape of a street, in region 2 processed by the geometric filter, as seen in Figure 29(G). In general, the residue of the restoration by the geometric filter contains some remainders of the original. In other words, most of the MSE error comes from edges or boundaries. The overall error however, is relatively small compared to that of the other methods, especially for this image degraded by moderate motion blur and a moderate noise level. Overall, our segmentation based approach gives better performance, in MSE sense, than the conventional approach of using same method for different segments. The result for the MAP method however gives lower LMSE value as seen in Figure 28(M).

Figure 30 contains the results for the restoration of Figure 22, in which the image is degraded by a combination of atmospheric blur and additive white noise

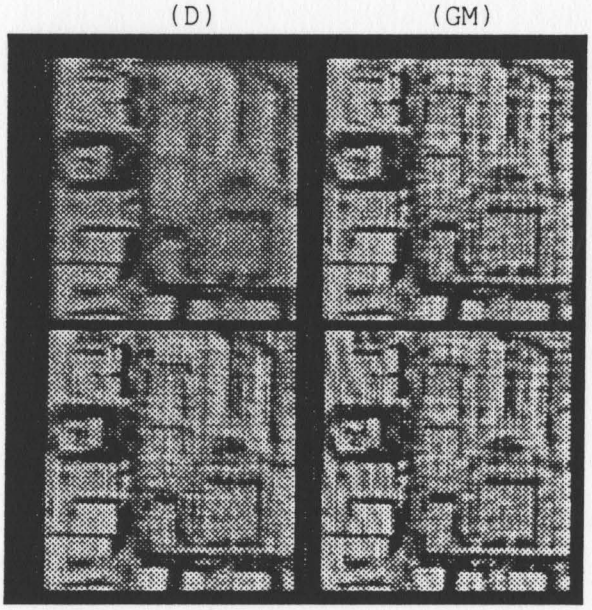

Figure 28. Restoration result of proposed approach on Figure 21.

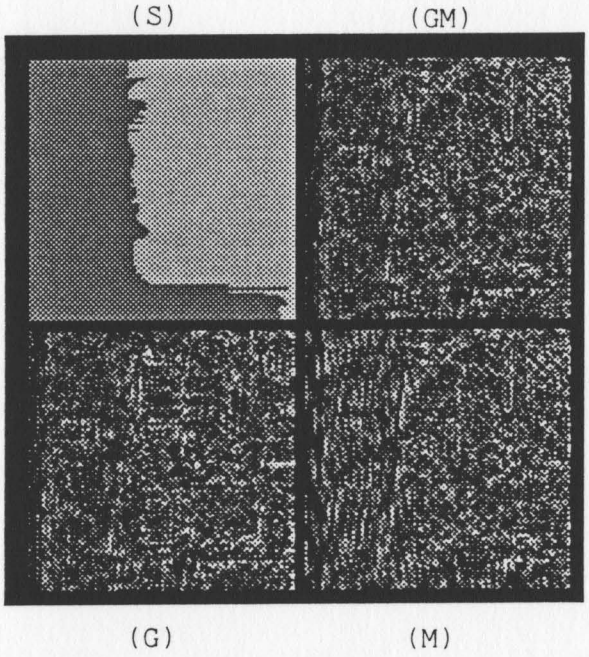

Figure 29. Illustration of residue images for Figure 28.

Table 5. Performance criteria for Figure 28.

Method A: Geometric Filter

	MSE	MAE	NMSE	NMAE	LOGMSE	LMSE	GMSE
Region 1	23.658	3.657	0.019	0.126	0.032	0.577	0.112
Region 2	43.085	5.165	0.027	0.136	0.008	0.894	0.245
Overall	33.909	4.453	0.024	0.132	0.017	0.740	0.173

Method B: MAP Method

	MSE	MAE	NMSE	NMAE	LOGMSE	LMSE	GMSE
Region 1	29.653	4.139	0.024	0.142	0.035	0.423	0.126
Region 2	37.353	4.846	0.023	0.128	0.006	0.529	0.240
Overall	33.716	4.512	0.024	0.134	0.018	0.478	0.179

Combined Method: Geometric Filter and MAP Method

	MSE	MAE	NMSE	NMAE	LOGMSE	LMSE	GMSE
Region 1	23.658	3.657	0.019	0.126	0.032	0.577	0.112
Region 2	37.353	4.846	0.023	0.128	0.006	0.529	0.240
Overall	30.885	4.284	0.022	0.127	0.017	0.552	0.171

of variance 25 in region 1, and motion blur and additive white noise of variance 16 in region 2. The selected method for region 1 is the MAP method (method A). The MAP method is powerful when images are degraded by atmospheric blur and very high noise (or low SNR). The Wiener filter (method B) is the choice of the expert system under the MSE sense for region 2 where it suffers from motion blur and high noise. The SNR value of region 1 and 2 is 10 dB and 14 dB respectively. As seen in Figure 31(W), the residue of the restoration by the Wiener filter shows some square patterns, especially in region 2. This error explains the smeared edges or boundaries in the restored image produced by the Wiener filter. This interpretation is confirmed in Table 6, where the LMSE error in region 2 is smaller by the MAP method than by the Wiener filter. For region 1, the MAP method outperforms the Wiener filter in terms of all error criteria. Overall, the combined method resulted in better performance than the conventional approach of using a single method for different segments of the image. The restoration by the MAP method however, gave smaller LMSE value which can be confirmed by Figure 30(M) and Table 6.

Figure 32(D) is synthesized by mixing two degraded images according to the predefined segmentation given in Figure 33(S). Reference back to Section 6.2 for details of synthesis. Natural test images of this shape and combination were not obtained during this study. This situation is the same for the test image given in Figure 34(D). The outer region (region 1) is degraded by atmospheric blur and noise of variance 36. The inner region (region 2) is degraded by motion blur and noise of variance 9. The SNR values for region 1 and region 2 are 12 dB and 19

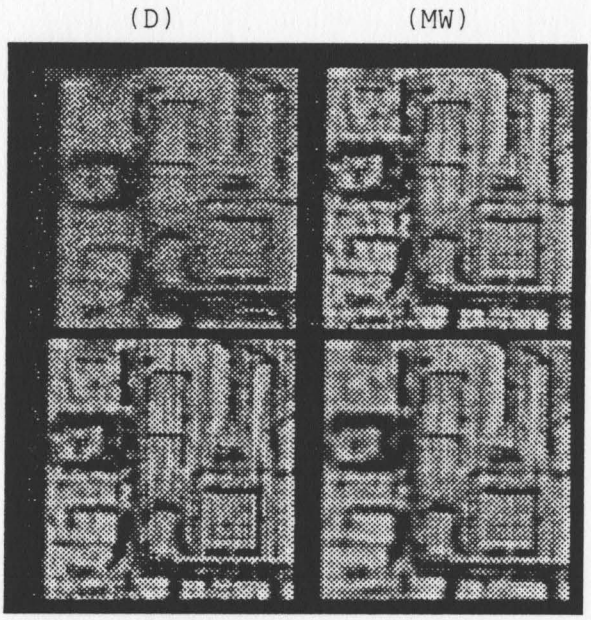

Figure 30. Restoration result of proposed approach on Figure 22.

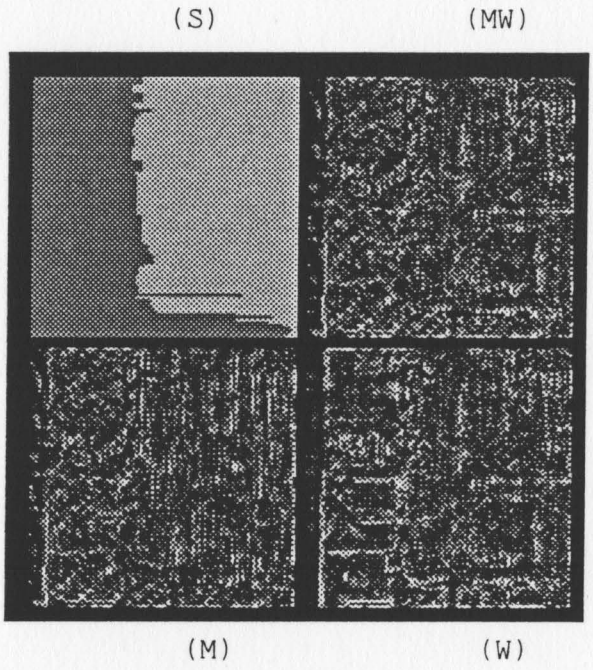

Figure 31. Illustration of residue images for Figure 30.

Table 6. Performance criteria for Figure 30.

Method A: MAP Method

	MSE	MAE	NMSE	NMAE	LOGMSE	LMSE	GMSE
Region 1	32.231	4.271	0.025	0.143	0.031	0.357	0.168
Region 2	34.343	4.629	0.022	0.125	0.008	0.513	0.216
Overall	33.377	4.465	0.023	0.132	0.017	0.442	0.191

Method B: Wiener Filter

	MSE	MAE	NMSE	NMAE	LOGMSE	LMSE	GMSE
Region 1	41.687	4.673	0.032	0.156	0.035	0.850	0.205
Region 2	27.089	4.018	0.017	0.109	0.008	0.617	0.164
Overall	33.770	4.318	0.024	0.128	0.019	0.723	0.185

Combined Method: MAP Method and Wiener Filter

	MSE	MAE	NMSE	NMAE	LOGMSE	LMSE	GMSE
Region 1	32.231	4.271	0.025	0.143	0.031	0.357	0.168
Region 2	27.089	4.018	0.017	0.109	0.008	0.617	0.164
Overall	29.443	4.133	0.021	0.122	0.017	0.500	0.165

dB respectively. For region 1, where atmospheric blur and low SNR exists, the MAP method is the choice of the expert system under the MSE criterion as stated previously. The selected method for region 2 is the geometric filter. As seen in Figure 33 and Table 7, the error between the two selected methods is small in region 2, about 1.3. This is partly because the SNR in this region is relatively high. For region 1, the MAP method outperforms the geometric filter with a big margin. Overall, the combined method resulted in a better restoration than either single method in MSE sense.

Figures 34 and 35 illustrate the restoration results for an image degraded by a combination of out-of-focus blur in the upper portion of the image (region 1) and severe motion blur in the lower portion (region 2). The SNR is about 17 dB for each region. The geometric filter is chosen by the expert system under the MSE criterion for region 1 and the MAP method is the choice for region 2. As can be seen in Table 8, the MSE difference for region 1 between these two methods is about 14. As discussed earlier, the restoration result by the geometric filter gets its MSE error mostly from the boundaries. This can be verified in Figure 35-c by examining the bright square patterns. The MAP method however, results in evenly distributed errors. Figure 35(M) confirms this observation. The MSE difference between the two methods for region 2 is small. We see however, relatively high MSE values for this region. Severe motion blur often results in high MSE values. Overall, the quality of the restoration result by the proposed approach is better than that of the conventional approach of using a single method. The subjective criteria however, would prefer Figure 34(G) to Figure

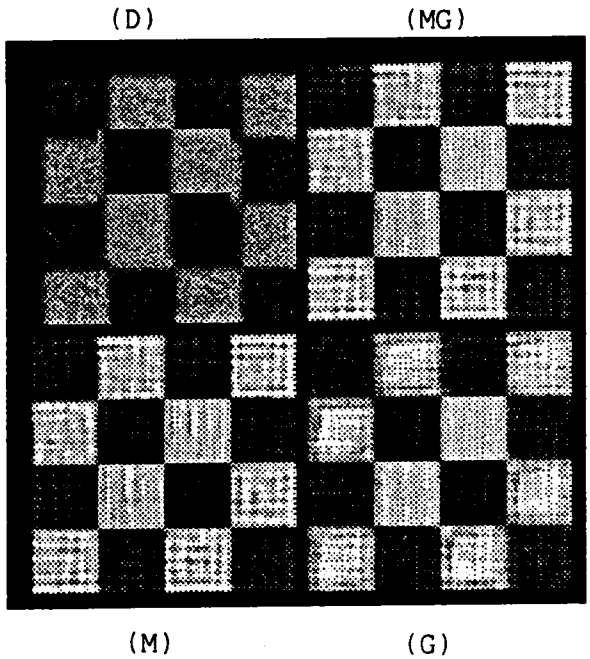

Figure 32. Restoration result of proposed approach on Figure 23.

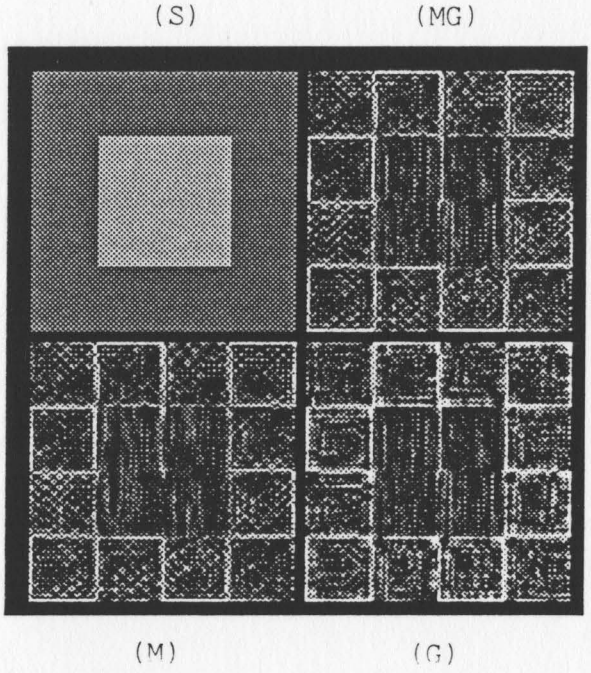

Figure 33. Illustration of residue images for Figure 32.

Table 7. Performance criteria for Figure 32.

Method A: MAP Method

	MSE	MAE	NMSE	NMAE	LOGMSE	LMSE	GMSE
Region 1	53.590	5.427	0.019	0.113	0.003	0.896	0.786
Region 2	18.069	3.348	0.006	0.070	0.001	0.383	0.163
Overall	44.709	4.907	0.016	0.102	0.002	0.718	0.576

Method B: Geometric Filter

	MSE	MAE	NMSE	NMAE	LOGMSE	LMSE	GMSE
Region 1	78.064	6.625	0.027	0.138	0.004	1.110	0.616
Region 2	16.782	3.080	0.006	0.064	0.001	0.382	0.175
Overall	62.743	5.739	0.022	0.120	0.003	0.857	0.467

Combined Method: MAP Method and Geometric Filter

	MSE	MAE	NMSE	NMAE	LOGMSE	LMSE	GMSE
Region 1	53.590	5.427	0.019	0.113	0.003	0.896	0.786
Region 2	16.782	3.080	0.006	0.064	0.001	0.382	0.175
Overall	44.388	4.840	0.015	0.101	0.002	0.717	0.584

34(GM). This speculation is confirmed by comparing LMSE or GMSE values between them. If we had wanted the restoration results to be best in perception sense, and the expert system were operating under say the LMSE instead of the MSE criterion, the system would have selected the geometric filter for both regions. This selection however, would have resulted in a restoration with a higher MSE.

In all of the examples given in this section, the restoration was oriented to accomplish minimum MSE. We obtained this goal as can be seen in Tables 5 through 8. We would like to point out however, that the combined methods suggested by our approach do not have to be different. Depending on the combination of blur type, noise level, and severity of blur in each region, the method chosen by the expert system under a given criterion, could be the same for each region.

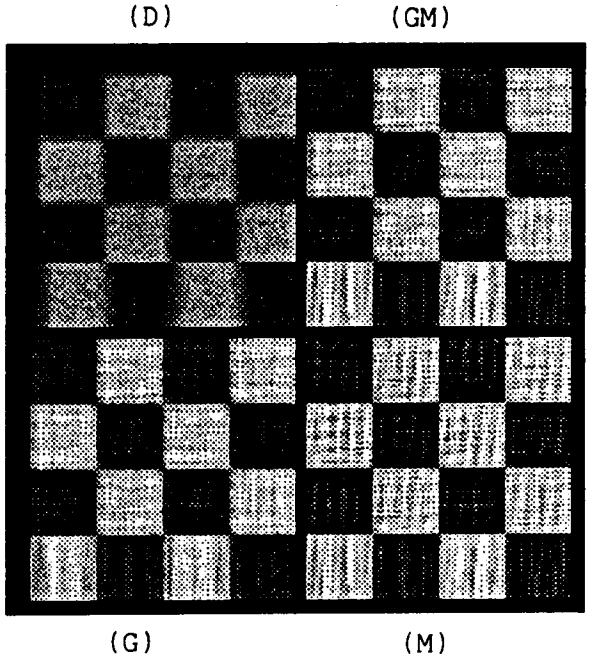

Figure 34. Restoration result of proposed approach on Figure 24.

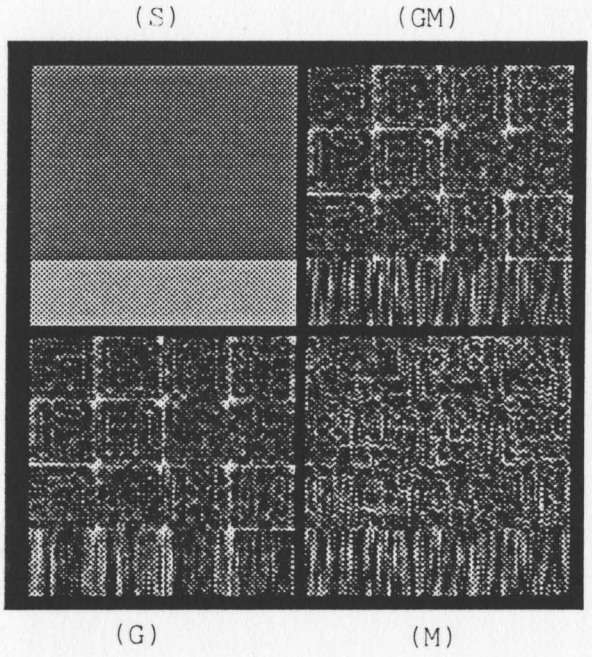

Figure 35. Illustration of residue images for Figure 34.

Table 8. Performance criteria for Figure 34.

Method A: Geometric Filter

	MSE	MAE	NMSE	NMAE	LOGMSE	LMSE	GMSE
Region 1	28.952	4.129	0.010	0.086	0.002	0.554	0.275
Region 2	45.061	5.447	0.016	0.113	0.003	0.520	0.360
Overall	32.979	4.458	0.011	0.093	0.002	0.547	0.292

Method B: MAP Method

	MSE	MAE	NMSE	NMAE	LOGMSE	LMSE	GMSE
Region 1	42.420	5.230	0.015	0.109	0.003	0.910	0.495
Region 2	38.919	5.056	0.014	0.105	0.003	0.683	0.470
Overall	41.544	5.187	0.014	0.108	0.003	0.864	0.490

Combined Method: Geometric Filter and MAP Method

	MSE	MAE	NMSE	NMAE	LOGMSE	LMSE	GMSE
Region 1	28.952	4.129	0.010	0.086	0.002	0.554	0.275
Region 2	38.919	5.056	0.014	0.105	0.003	0.683	0.470
Overall	31.443	4.361	0.011	0.091	0.002	0.580	0.315

Chapter VII. Conclusions and Suggestions

7.1 Conclusions

It is safe to say that there is no image processing without involving image restoration. Accordingly, extensive research has been reported during the last two decades. There is however, no general image restoration method available. Although numerous image restoration methods have been proposed, none of the methods can handle all the kinds of degradation which subject images can suffer. Also the usual assumption of a single degradation characterization for the whole image is not correct in general. As a consequence, it is a better idea to segment the image into a number of homogeneous regions and to apply different restoration methods for each of the regions.

The proposed image restoration method, which is supported by a rule-based expert system, attends to the above problems. The necessity and importance of the proposed system has been addressed by researchers in the image restoration field for some time [2, 3]. To the best of our knowledge however, no research work in this direction has been reported. We emphasized that the actual implementation of our system involves two very unrelated fields: artificial intelligence, and image restoration.

The performance of the knowledge system presented in this dissertation was evaluated by computer simulations on both real and simulated images. In addition to the quantitative evaluations of the restored images, subjective comparisons were carried out by computing several semi-qualitative measures.

The results of the experiments in Section 6.5 illustrate that the approach of the proposed system, with segmentation and restoration of individual segments, performs better than conventional approaches.

The merits of our expert system are fourfold:

1. Versatility - The system incorporates several image restoration methods. Each method is designed to treat a specific case; for example in the MSE sense, the geometric filter is the choice when degradation is caused by motion blur with low to medium noise or MAP is good for images degraded by atmospheric blur with severe noise. With the help of an expert system, all methods implemented in the system are combined into a general tool which can treat virtually any kind of image degradation.

2. Generality - By adapting the image segmentation approach, the conventional approaches such as categories (1), and (3) of Chapter III can be implemented by our system as special cases.
3. Better performance - By applying a properly selected image restoration method for each of the segmented regions, the overall performance was shown to be better than that of using a single method for the whole image, either in the MSE sense or in the human perception sense.
4. Modularity/Expandability - Each part of the proposed system is inter-related only by the interface module. Each module can be expanded or modified independently without affecting other parts of the system. The A.I. module or the computational module can be expanded easily as the requirements of the system grow.

7.2 Limitations and Their Significance

It is possible to obtain an incorrect impression about the extent to which image restoration can be carried out. Hunt [3, p.74] makes assertions about the practical solution of image restoration problems as follows:

> " ... assertions that are offered with no proofs but which have grown out of the author's experience in this area ... If an image restoration problem can be solved, then about 75 percent of the time it can be treated with some of the simplest techniques, for example, inverse or Wiener filter. Of the 25 percent of cases not solved by simpler techniques, perhaps only half of these will be amenable to solutions by a complex technique. There remains a core of problems that can not be solved by any method of image restoration ... "

The test images we have processed in Section 6.5, Figures 21 through 24, are among the ones that can not be solved properly so far. In that sense, we have reduced the percentage of unsolvable problems, which represents the significance of this study.

The restoration methods implemented in this dissertation exploited FFT techniques extensively. Most of the computations are performed in the frequency domain, which means that linear convolutions are approximated by circular convolutions. As a consequence, we lose information when a segmented region is processed with a filter impulse response with larger support than the border of zeros surrounding the segment. Such occurrence should be avoided, or controlled.

Since the test images are synthesized artificially by combining two different images, pixels on opposite sides of the boundary do not have any interaction with each other. The overlap-and-save algorithm should then not be applied.

We assumed that motion blur is horizontal. Motion blur under α degrees can not be estimated by the present system. We also assumed that the PSF is symmetric. Images suffering from asymmetric degradation can not be restored unless we have exact values of the PSF array.

7.3 Future Directions

The encouraging results obtained in this endeavor suggest the need for extending the idea to other areas of image processing. In particular, image en-

hancement schemes may be added to the system to facilitate a wider range of applications.

As for the system itself, the following features are considered necessary to widen the capability of the system.

1. To decide a proper threshold for image segmentation, the addition of a histogram generation and display capability would be useful.
2. To make the system more versatile, more special purpose image restoration methods may be added to the system. The addition of image restoration methods for multi-channel images would be a good candidate for extension. To treat X-ray images, a restoration method for stochastically degraded images [112] is also desirable.
3. To be of more practical use, the ability to display results on the display interactively would be desirable. Real time processing by incorporating custom-made hardware into the system, may be worth pursuing. Especially for military applications, this could be desirable.

References

1. B. Hunt, "Bayesian Methods in Nonlinear Digital Image Restoration", *IEEE Trans. Computer, Vol. C-26 No. 3,* 219-229, Mar. 1977.

2. H. Andrews and B. Hunt, *Digital Image Restoration,* Prentice-Hall, 1977.

3. M.P. Ekstrom (Ed), *Digital Image Processing Techniques,* Academic Press, 1984.

4. T. Kailath (Ed.), *Modern Signal Processing, Chapter 9,* Hemisphere Publishing Corporation, 1985.

5. R. Kasturi, *Adaptive Image Restoration in Signal-Dependent Noise,* Ph.D. Dissertation, Texas Tech, 1982.

6. T.S. Huang (Ed.), *Advances in Computer Vision and Image Processing, Chapter 6, (Volume 1): Image Reconstruction from Incomplete Observations,* Connecticut: JAI Press Inc, 1984.

7. T.S. Huang (Ed.), *Advances in Computer Vision and Image Processing, Chapter 5, (Volume 2): Image Enhancement & Restoration,* Connecticut: JAI Press Inc, 1986.

8. R. Gonzalez and P. Wintz, *Digital Image Processing (2nd Edition),* Addison Wesley, 1987.

9. A. Rosenfeld and A. Kak, *Digital Image Processing (2nd Edition), Vol.1,* Academic Press, 1982.

10. K. Castleman, *Digital Image Processing,* Prentice-Hall, 1979.

11. J. Moik, *Digital Processing of Remotely Sensed Images,* NASA SP-431, NASA, 1980.

12. W. Pratt, *Digital Image Processing,* John Wiley & Sons, Inc., 1978.

13. E. Hall, *Computer Image Processing & Recognition,* Academic Press, 1979.

14. T.Huang (Ed.), *Picture Processing & Digital Filtering,* Springer-Verlag, 1975.

15. P. Harman & David King, *Expert Systems,* John Wiley & Sons, Inc., 1975.

16. R. Forsyth (Ed.), *Expert Systems: Principles & Case Studies,* Chapman & Hall, 1984.

17. J. Chassery, "Expert Systems & Image Processing," *Image Analysis & Processing,* V. Cantoni(Ed.), Plenum Press, 1985.

18. M. Nagao, "Strategies For Human-Like Image Understanding Systems", *Proceedings of Cognitiva,* CESTA, Paris, 1985.

19. T. Matsuyama, "Knowledge Organization & Control Structure in Image Understanding", *Proceedings of 7th ICPR,* 1118-1127, IEEE Computer Society Press, 1984.

20. J. Tsotsos, "Knowledge Of the Visual Process: Content, Form, & Use", *Proceedings of 6th ICPR,* 654-669, IEEE Comp. Soc. Press, 1982.

21. A. Nozit & M. Levine, "Low Level Image Segmentation: An Expert System", *IEEE Trans PAMI, Vol. 6,* 555-577, 1984.

22. K. Fu & J. Mui, "A Survey on Image Segmentation", *Pattern Recognition, Vol. 13,* 3-16, Pergamon Press, 1981.

23. A. Rosenfeld, "Image Analysis: Problems, Progress & Prospects", *Pattern Recognition, Vol. 17, No. 1,* 3-12, Jan., 1984.

24. R. Haralick and L. Shapiro, "Survey, Image Segmentation Techniques," *Computer Vision, Graphics, & Image Processing, Vol. 29,* 100-132, 1985.

25. A. Rosenfeld, "Picture Processing: 1986", *Computer Vision, Graphics, & Image Processing, Vol. 31,* 1987 (Also annually from 1972 through 1986).

26. R. Haralick, "Boundary Delineation & Image Segmentation" *EE 5510, Computer Vision Class Notes,* Winter Quarter, 1984.

27. S. Horowitz & T. Pavlidis, "Picture Segmentation By A Tree Traversal Algorithm", *J. Assoc. Computer, Vol. 23,* 368-388, 1987.

28. D. Jeong, *Unified Approach for the Early Understanding of Images,* M.S. Thesis, Virginia Polytechnic Institute and State University, May 1985.

29. D. Jeong & P. Lapsa, "Unified Approach for Low Level Image Analysis," *Proceedings of ICASSP 87,* 579-582, Dallas, Texas, April 1986.

30. J. Gilmore, "Artificial Intelligence In Image Processing", *Proceedings of SPIE, Vol. 528. (A. Tesher, Ed.),* 192-201, L.A., California, Jan. 1985.

31. R. Haralick, "Edge and Region Analysis for Digital Image Data," *Comp. Graphics and Image Processing,* Vol. 12, 60-73, 1980.

32. H. Andrews, "Digital Image Restoration: A Survey", *Computer, Vol. 7,* 36-45, May. 1974.

33. B. Frieden, "Image Enhancement & Restoration", *Picture Processing & Digital Filtering, T. Huang (Ed.),* Chap. 5., Springer-Verlag, Berlin, 1975.

34. G. Anderson and A. Netravali, "Image Restoration Based On A Subjective Criterion", *IEEE. SMC, Vol. 6.* 845-853, 1976.

35. S. Rajala & R. Figueiredo, "Adaptive Non-Linear Image Restoration By A Modified Kalman Filtering Approach" *IEEE ASSP-29 (5),* 1033-1042, Oct. 1981.

36. M. Sondhi, "Image Restoration : The Removal Of Spatially Invariant Degradations", *Proceedings of IEEE, Vol. 60, No. 7,* 842-853, July 1972.

37. R. Kasturi & J. Walkup, "Nonlinear Image Restoration" *Proceedings of SPIE (A. Tesher, Ed.), Vol. 528,* 43-61, January 1985.

38. A. Sawchuk, "Space-Variant Motion Degradations" *Proceedings of IEEE, Vol. 60, No. 7,* 854-861, July 1972.

39. G. Robbins, "Image Restoration For A Class Of Linear Spatially-Variant Degradations", *Pattern Recognition, Vol. 2, No. 2,* 91-105, 1970.

40. G. Robbins & T. Huang, "Inverse Filtering For Linear Shift-Variant Imaging Systems" *Proceedings of IEEE, Vol. 60, No. 7,* 862-872, 1972.

41. S. Kawata & Y. Ichioka, "Iterative Image Restoration for Linearly Degraded Images," *JOSA, Vol. 70, No. 7,* July 1980.

42. N. Nahi, "Role of Recursive Estimation in Statistical Image Enhancement," *Proceedings of IEEE, Vol. 60, No. 7,* 872-877, 1972.

43. E. Angel & A. Jain, "Restoration of Images Degraded by Spatially Varying PSF by a Conjugate Gradient Method," *Appl. Opt., Vol. 17,* 2186-2190, 1978.

44. J. Woods & L. Radewon, "Kalman Filtering in Two Dimensions," *IEEE IT-23(4),* July 1977.

45. B. Hunt & H. Trussell, "Sectioned Methods for Image Restoration," *IEEE ASSP-26(2),* 157-164, April, 1978.

46. A. Aboutalib & L. Silverman, "Restoration Of Motion Degraded Images," *IEEE CAS-22(3),* 278-286, March 1975.

47. L. Han & W. Yenping, "A New Model of Motion Blurred Images and Estimation of Its Parameters," *Proceedings of ICASSP 86, Tokyo Japan, April 1986.*

48. A. Aboutalib, M. Murphy, & L. Silverman, "Digital Restoration Of Images Degraded By General Motion Blurs", *IEEE AC-22,* 294-302, June, 1977.

49. A. Lohman & D. Paris, "Space-Variant Image Formation," *JOSA Vol. 55,* 1007-1013, 1965.

50. T. Katayama, "Restoration of Images Degraded by Motion Blur and Noise," *IEEE AC-27(5),* 1024-1033, Oct. 1982.

51. J. Goodman, *Introduction To Fourier Optics,* McGraw-Hill, New York, 1968.

52. R. Hufnagel & N. Stanley, "Modulation Transfer Function Associated With Image Transmission Through Turbulent Media", *JOSA-54,* 52-61, 1964.

53. B. McGlamery, "Restoration of Turbulence Degraded Image", *JOSA-57,* 293-297, Mar. 1967.

54. J. Walkup & R. Choens, "Image Processing in Signal Dependent Noise", *Optical Engineering,* Vol. 13, No. 3, 258-266, 1974.

55. S. Powell & L. Silverman, "Modeling of Two-Dimensional Covariance Functions with Application to Image Restoration," *IEEE AC-19(1)*, 8-13, Feb. 1974.

56. A. Netravali & B. Brasada, "Adaptive Quantization of Picture Signals Based On Spatial Masking", *Proc. IEEE,* Vol. 65, 536-548, Apr. 1977.

57. H. Jinchi, T. Simchony, & R. Chellappa, "Stochastic Relaxation For MAP Restoration of Gray Level Images with Multiplicative Noise", *ICASSP 87,* 28.16.1-4, 1236-1239, Dallas Texas, April 1987.

58. J.Qian, K-B. Yu, & R. Haralick, "A Multi-Threshold Adaptive Filtering For Image Enhancement", *ICASSP 86, 46.6.1.-4,* 2467-70, Tokyo Japan, April 1986.

59. A. Oppenheim & R. Schafer, *Digital Signal Processing,* Prentice-Hall, 1975.

60. S. Nakamori, "On-line Identification of Time Variant Parameters Using Covariance Information," *ICASSP 86,* 2723-6, Tokyo Japan, April 1986.

61. J. Biemond, F. Putten, & J. Woods, "Identification and Restoration of Images with Symmetric Noncausal Blurs," *IEEE Trans. Circuits and Systems,* To appear.

62. A. Tekalp, H. Kaufman, & J. Woods, "Identification of Image and Blur Parameters for Restoration of Noncausal Blurs," *IEEE ASSP-34(4),* 963-972, Aug. 1986.

63. T. Stockham, T. Cannon, & R. Ingebretsen, "Blind Deconvolution Through Digital Signal Processing," *IEEE Proc. Vol. 63 (4),* April 1975.

64. T. Cannon, H. Trussell, & B. Hunt, "Comparison of Image Restoration Methods," *Applied Optics, Vol. 17 (21)* Nov. 1978.

65. C. Helstrom, "Image Restoration by the Method of Least Squares", *JOSA, Vol. 57, No. 3,* 297-303, Mar. 1967.

66. B. Hunt, "The Application of Constrained Least Squares Estimation to Image Restoration by Digital Computer," *IEEE Trans. Computer, Vol. C-22 (9),* 805-812, Sept. 1973.

67. B. Hunt, "Digital Image Processing", *Proceedings of IEEE, Vol. 63, No. 4,* April, 1975.

68. B. Frieden, "Restoring with Maximum Likelihood and Maximum Entropy", *JOSA, Vol. 62, No. 4,* 511-518, April, 1972.

69. A. Albert, *Regression, and the Moore-Penrose Pseudo Inverse,* Academic Press, New York, 1972.

70. Y. Ichioka, Y. Takubo, K. Matsuoka, & T. Suzuki, "Iterative Image Restoration by the Method of Steepest Descent", *Journal of Optics, Vol. 12, No. 1,* 34-41, Jan/Feb. 1981.

71. S. Kawata & Y. Ichioka, "Iterative Image Restoration for Linearly Degraded Images: I. Basis", *JOSA, Vol. 70, No. 7,* July, 1980.

72. R. Schafer, R. Mersereau, & R. Richards, "Constrained Iterative Restoration Algorithms", *Proceedings of IEEE, Vol. 69, No. 4,* 432-450, April, 1981.

73. S. Singh, S. Tandon, & H. Gupta, "An Iterative Restoration Technique", *Signal Processing, Vol. 11,* 1-11, Jan., 1986.

74. H. Trussell, "Convergence Criteria for Iterative Restoration Methods", *ASSP-31 (1)* 129-136, Feb. 1983.

75. H. Van Trees, *Detection, Estimation, & Modulation Theory,* Vol. 1, New York; Wiley, 1968.

76. H. Trussell & B. Hunt, "Improved Methods of Maximum A Posteriori Restoration", *IEEE Trans. on Comp. Vol. C-27, No. 1,* 57-62, Jan. 1979.

77. E. Isaacson & H. Keller, *Analysis of Numerical Methods,* New York; Wiley, 1966.

78. H. Trussell, "The Relationship Between Image Restoration by the MAP Method and a Maximum Entropy Method," *ASSP-28 (1),* 114-117, Feb. 1980.

79. N. Nahi & T. Assefi, "Bayesian Recursive Image Estimation", *IEEE Trans. Computer, Vol. C-21,* 734-738, July 1972.

80. J. Woods, & V. Ingle, "Kalman Filtering in Two Dimensions: Further Results," *IEEE Trans. ASSP-29(2),* 188-196, April 1972.

81. J. Biemond, J. Rieske, & J. Gerbrands, "A Fast Kalman Filter for Images Degraded by Both Blur And Noise," *IEEE Trans. ASSP-31(5),* 1248-1256, Oct. 1983.

82. M. Watanabe, E. Osoki, S. Horii, & S. Kageyama, "A New Recursive Estimation Method for Digital Image Restoration and Its Applications," *Proc. ICASSP 86,* 2475-2478, Tokyo Japan, April 1986.

83. J. Min & C. Xian, "A New Approach to 2-D Kalman Filtering," *Proc. ICASSP 87,* 1232-1235, Dallas Texas, April, 1987.

84. A. Jain & J. Jain, "Partial Differential Equations & Finite Difference Methods in Image Processing, Part 2: Image Restoration," *IEEE Trans. AC-23(5),* 817-834, Oct. 1978.

85. D. Youla & H. Webb, "Image Restoration by the Method of Convex Projections: Part 1-Theory," *IEEE Trans. Medical Imaging, Vol. ME-1(2),* 81-94, Oct. 1982.

86. M. Sezan & H. Stark, "Image Restoration by the Method of Convex Projections: Part 2- Applications and Numerical Results," *IEEE Trans. Medical Imaging, Vol. ME-1(2),* 95-101, Oct. 1982.

87. M. Sezan & H. Stark, "Image Restoration by Convex Projections in the Presence of Noise," *Appl. Optics, Vol. 22, No. 18,* 2781-2789, Sep. 1983.

88. D. Felix, P. Cheng, & G. DeMoment, "Image Deconvolution Using 2-D Noncausal Fast Kalman Filter," *Proc. ICASSP 86,* Tokyo Japan, April 1986.

89. H. Trussell & M. Civanlar, "Feasible Solution in Signal Restoration," *IEEE Trans. ASSP-32(2),* 201-212, April 1984.

90. H. Trussell & M. Civanlar, "The Initial Estimate in Constrained Iterative Restoration", *ICASSP 1983,* 643-646, Boston MA., April 1983.

91. R. Leahy & C. Goutis, "An Optimal Technique for Constraint-Based Image Restoration and Reconstruction," *IEEE ASSP-34(6),* 1629-1642, Dec. 1986.

92. M. Civanlar, & H. Trussell, "Digital Signal Restoration Using Fuzzy Sets," *IEEE Trans. ASSP-34(4),* 919-936, Aug. 1986.

93. A. Kandel & W. Byatt, "Fuzzy Sets, Fuzzy Algebra & Fuzzy Statistics", *Proceedings of IEEE, Vol. 66, No. 12,* 1619-1639, December, 1978.

94. D. Dubois & H. Prade, *"Fuzzy Sets and Systems: Theory & Applications",* New York: Academic Press, 1978.

95. S. Kardo & K. Atsuta, "Constrained Generalized Inverse Matrix," *Proceedings of ICASSP 86,* Tokyo Japan, April 1986.

96. B. Tatian, "Methods for Obtaining the Transfer Function From the Edge Response Function," *JOSA, Vol. 55, No. 8,* 1014-1019, Aug. 1965.

97. C. McGillem, P. Anuta, E. Malaret, & K-B. Yu, "Estimation of a Remote Sensing System Point-Spread-Function from Measured Imagery", *9th International Symposium on Machine Processing of Remote Sensed Data,* West Lafayette, Ind., June 1983.

98. J. Biemand, F. Putten, & J. Woods, "A Parallell Identification Procedure for Images with Noncausal Symmetric Blurs," *Proc. ICASSP 86,* Tokyo Japan, April 1986.

99. D. Graupe, D. Krause, & J. Moore, "Identification of ARMA Parameters of Time Series," *IEEE Trans. AC-20(1),* Feb. 1975.

100. J. Bescos, I. Glaser, & A. Sawchuk, "Restoration of Color Images Degraded by Chromatic Aberrations", *Applied Optics, Vol. 19 (22),* 3869-3876, Nov. 1980.

101. J. Bescos, J. Altamira, J. Santamar, and A. Santiste, "Restoration of Defocusing & Chromatism in Color Images", *SPIE, Vol. 359,* 242-248, 1982.

102. N. Galatsanos & R. Chin, "Digital Restoration of Multi-Channel Images," *Proc. ICASSP 87,* 1244-1247, Dallas Texas, April 1987.

103. B. Hunt & O. Kubler, "Karhunen-Loeve Multispectral Image Restorations, Part 1: Theory," *IEEE Trans. ASSP-32 (3),* 592-600, June 1984.

104. D. Angwin, & H. Kaufman, "Effect of Modeling Domains on Recursive Color Image Restoration," *Proc. ICASSP 87,* 1229-1232, Dallas Texas, April 1987.

105. A. Katsaggelos, "Multiple Input Adaptive Iterative Image Restoration Algorithms," *Proc. ICASSP 87,* 1179-1182, Dallas Texas, April 1987.

106. D. Ghiglia, "Space Invariant Deblurring Given N Independently Blurred Images of a Common Object", *JOSA, Vol. 74,* 398-402, 1984.

107. W. Saxton, *Computer Techniques for Image Processing in Electron Microscopy,* Academic Press, 1978.

108. A. Katsaggelos & R. Schafer, "Iterative Deconvolution Using Different Distorted Versions of an Unknown Signal", *Proc. ICASSP 83,* 659-662, Boston MA, April 1983.

109. M. Hayes, J. Lim, & A. Oppenheim, "Signal Reconstruction from Phase or Magnitude", *IEEE Trans, ASSP, Vol. 28,* 672-680, 1980.

110. M. Hayes, "The Reconstruction of a Multidimensional Sequence from the Phase or Magnitude of its Fourier Transform", *IEEE Trans. ASSP, Vol. 30,* 140-154, 1982.

111. C-T. Chen, M. Sezan, & A. Tekalp, "Effects of Constraints, Initialization, and Finite-Word Length in Blind Deblurring of Images by Convex Projections," *Proc. ICASSP 87,* 1201-1204, Dallas Texas, April 1987.

112. H. Trussell & P. Combettes, "Considerations for the Restoration of Stochastic Degradations," *Proc. ICASSP 87,* 1209-1212, Dallas Texas, April 1987.

113. N. Otsu, "Multiple-Regression Analysis Approach to Automatic Design of Adaptive Image Processing Systems," *SPIE, Vol. 435,* 70-75, 1983.

114. C. Hall, "Subjective Evaluation of a Perceptual Quality Metric," *Proc. SPIE, Vol. 310,* 200-204, 1981.

115. A. Habibi, "Two-Dimensional Bayesian Estimate of Images," *Proc. IEEE, Vol. 60, No. 7,* 878-883, July 1972.

116. D. Jameson & L. Hurvich (Ed.), *Visual Psychophysics,* Springer-Verlag, 1972.

117. J. Kowalik (Ed.), *Knowledge Based Problem Solving,* Prentice-Hall, 1986.

118. C. Hall, "Subjective Evaluation of a Perceptual Quality Metric," *Proc. SPIE, Vol. 310,* 200-204, 1981.

119. A. A. (Louis) Beex, "Iterative Reconstruction of Space-Limited Scenes from Noisy Frequency-Limited Measurements," *Proc. ICASSP 83,* 147-150, Boston, Mass. April 1983.

120. A. A. (Louis) Beex, "Soft Constraint Iterative Reconstruction from Noisy Projections," *Proc. ICASSP 84,* 12A.6.1-4, San Diego, CA. March 1984.

Appendix A. Sample Terminal Session

```
$ RUN ZEBRA

ENTER THE NAME OF DEGRADED IMAGE, g(x,y)
GB

DO YOU WANT THE SUBJECT IMAGE TO BE SEGMENTED?
TYPE Y FOR YES, N FOR NO.
N

THIS IS FOR REGION NUMBER ...                1

DO YOU NEED TO COMPUTE A POSTERIORI INFORMATION?
TYPE Y FOR YES, N FOR NO.
N

WE NOW PROCESS THE BLOCK WITH COORDINATES AS
ROW FROM              1    ...      TO            128
COLUMN FROM              1   ...     TO             128

ENTER NAME OF THE PSF ARRAY FOR THIS BLOCK.
HB

PLEASE SPECIFY THE TYPE OF PSF...
(MOT: MOTION, OOF: OUT-OF-FOCUS, ATM: ATMOSPHERIC)
MOT

ENTER THE NAME OF NOISE ARRAY, n(x,y).
NB

DO YOU WANT THE HELP OF AN EXPERT SYSTEM
TO DECIDE THE PROPER RESTORATION METHOD?
TYPE Y FOR YES, N FOR NO.
N

SELECT ONE OR TWO METHODS FROM THE FOLLOWINGS.

WIENER FILTER(MMSE) ..................  1
HOMOMORPHIC FILTER(PSE) ..............  2
MAXIMUM ENTROPY METHOD(LINEARIZED) ..  3
GEOMETRIC/INVERSE  FILTER ............  4
CONSTRAINED LEAST SQUARE METHOD .....  5
MAP METHOD ...........................  6

HOW MANY METHODS DO YOU WANT TO SELECT (MAX.  2)?
1

ENTER THE NUMBER OF YOUR FIRST CHOICE.
6

DO YOU WANT TO READ INTO THE ORIGINAL IMAGE,
RATHER THAN ESTIMATE FROM THE DEGRADED IMAGE? (Y OR N)
N
```

(Appendix A continues)

```
LET US ESTIMATE THE SPECTRUM OF ORIGINAL
WITH AVAILABLE INFORMATIONS. . .

********** ENTERING MAP METHOD ********

MMR AND MMC VALUES ARE. . .                    7              7
VARIANCE AND NORM OF NOISE . . .    9.160583          150087.0


ITERATION NUMBER & DIFFERENCE ARE. .                1    108430.0

DIFFERENCE IS SMALL ENOUGH AT ITERATION. .                      1
MINIMUM AND MAXIMUM GRAY VALUES. .   -12.79417          66.84731
 ------- EXIT FROM MAP ------


WE NOW NEED AN ORIGINAL IMAGE TO COMPUTE PERFORMANCE.
ENTER THE NAME OF ORIGINAL. . .
OG

THE NUMBER OF PIXELS PROCESSED. . .          16384

THE QUALITY MEASURE OF THIS REGION . . .

MSE=    12.45612          MAE=    2.387268
NMSE=   1.5431034E-02      NMAE=   0.1257034
LOGMSE=   6.3303925E-02     RMSSNR=    41.71375
ABSSNR=    20.73830          LMSE=   0.3989764
GMSE=   0.1048677

WITHIN PERFORMB (FOR WHOLE IMAGE). . .

MSE=    17.96517          MAE=    3.287001
NMSE=   1.2518902E-02     NMAE=   9.7357251E-02
LOGMSE=   1.2387450E-02     RMSSNR=    43.80516
ABSSNR=    23.29368
LMSE=   0.3896192      GMSE=   9.7836934E-02
GIVE NAME TO THE RESIDUAL IMAGE. .
RB-E-M

NAME THE DATA FILE OF THESE CRITERIA.
CB-E-M

NAME THE RESTORED IMAGE.
GB-E-M

MINIMUM AND MAXIMUM GRAY VALUES. .   0.0000000E+00    66.84731

FOR DISPLAYING PURPOSE, POWER OF OUTPUT CAN BE ADJUSTED
TO THAT OF THE ORIGINAL.  WANT IT? (Y OR N)
Y

DO YOU WANT TO PROCESS THIS SAME IMAGE
WITH DIFFERENT METHOD?  (Y OR N)
N

DO YOU HAVE ANOTHER DEGRADED IMAGE
TO BE PROCESSED? (Y OR N)
N
$ LOG
```

The vita has been removed from the scanned document